KU-18-1

Analytical Investigation of Saddle Connections for Overhead Sign Trusses with Respect to Strength and Fatigue Performance

By

Danqing Yu, M.S.

Caroline Bennett, Ph.D., P.E.

Jian Li, Ph.D., P.E.

William Collins, Ph.D., P.E.

Elaina Sutley, Ph.D.

A Report on Research Sponsored by
The Kansas Department of Transportation

Structural Engineering and Engineering Materials
SM Report No. 144
August 2020

THE UNIVERSITY OF KANSAS CENTER FOR RESEARCH, INC.

2385 Irving Hill Road – Campus West, Lawrence, Kansas 66045

Executive Summary

Bridge-type overhead truss sign structures (OHTSS) are widely used over active highways across the states. An OHTSS is comprised of a 3D truss and two support frames at each end. The structures are usually made of steel or aluminum. Many state DOTs use their own types of connections that are not documented in specifications. Since 2015, the Kansas DOT has used a type of 'saddle connection' at the joints of truss chords and support frame pipes. Wind loads are the primary type of load a sign structure resists besides the gravity load. Since wind loads are periodic, fatigue properties are important in the design of OHTSS. As a newly developed connection, the Kansas DOT sought information regarding the mechanical performance of the saddle connection. Studies were needed to verify the safety of the connections, particularly regarding its fatigue susceptibility.

This report present a study mainly aimed at evaluating the fatigue susceptibility of the saddle connections using finite element analysis (FEA). The study consisted of the following four parts:

Part 1 - Global behavior analysis: an analysis aimed at determining the global behavior of the structures and the location of critical connections. Linear-elastic material properties were used.

Part 2 - Structural Hot Spot Stress analysis: an analysis was performed to determine structural Hot Spot Stresses along each weld in the critical connections identified in Part 1. Linear-elastic material properties were used.

Part 3 – Effective notch stress analysis: a linear-elastic analysis using the effective notch stress method to evaluate three welds identified to have larger stresses in Part 2. Linear-elastic material properties were used.

Part 4 – Extreme loading analysis: An analysis to evaluate the behavior of the saddle connections and the overall structures under extreme loading and provide comments regarding the strength-related safety of the saddle connections. Elastic-perfectly plastic material properties were used.

Sign structures of four span lengths, including 60 ft, 83 ft, 110 ft, and 137 ft, were analyzed in Part 1 and Part 2. The 137 ft span structure was analyzed in part three using the effective notch stress method. The 60 ft and 137 ft span structures were analyzed in part four.

In Parts 1 and 2, AASHTO fatigue loads, including natural wind gusts and truck-induced gusts, were applied in six load modes. They included: natural wind blowing from the back, front, and side of sign structures; and truck-induced gusts acting on the right, middle, and left 12 ft of sign trusses. In Part 3, the AASHTO fatigue load of the natural wind blowing from behind the sign structure was applied. In Part 4, the overall structures and the saddle connections were loaded until the analysis terminated. The termination of analysis was governed by loss of stiffness due to the yielding of material.

The study resulted in conclusions that the natural wind in the direction facing the sign panel almost always governed the fatigue demand. The bottom saddle connections were more susceptible to fatigue damage than the top saddle connections, especially the stiffener-to-pipe weld in the bottom saddle connection. Fatigue failures of the saddle connections are not likely to occur in expected real use, but attention should be paid to the stiffener-to-pipe weld in the bottom saddle connection. The analysis of the structures under extreme loading suggests that the ultimate strength of saddle connections do not govern the strength of the overall structures.

Acknowledgements

The authors of this report would like to gratefully acknowledge the Kansas DOT for their support of the work performed under the KTRAN project KU-18-1.

Contents

List of Figures 6
List of Tables 8
1. Background 9
1.1 Introduction of Saddle Connection 9
1.2 Fatigue Analysis Methods Using Finite Element Analysis 12
1.2.1 Nominal Stress Method 12
1.2.2 Structrual Hot Spot Stress Method 13
1.2.3 Effective Notch Stress Method 16
2. Objective and Scope 18
3. Part One: Evaluating Global Behavior of Structures and Determining Critical Connections 20
3.1 Model Introduction 20
3.2 Analysis Results 24
4. Part Two: Structural Hot Spot Stresses Analysis 28
4.1 Model Introduction 28
4.2 Analysis Results 32
5. Part Three: Effective Notch Stresses Analysis 36
5.1 Model Introduction 36
5.2 Analysis Results 40
6. Part Four: Behavior of Overhead Truss Sign Structure under Extreme Loading 44
6.1 Model Introduction 44
6.1.1 Behavior of Overall Structure 44
6.1.2 Performance of Saddle Connections 45
6.2 Analysis Results 47
6.2.1 Behavior of Overall Structure 47
6.2.2 Performance of Saddle Connections 49
7. Conclusions 56
Reference 58

List of Figures

Figure 1. Coupler Connection Traditionally Used on Aluminum Overhead Truss Sign Structures in Kansas 9
Figure 2. Saddle-Type Connections for Aluminum Overhead Truss Sign Structures 10
Figure 3. Fatigue Resistance S-N Curve of Steel Details for Hot Spot Stress Analysis 15
Figure 4. Fatigue Resistance S-N Curve of Steel Details for Effective Notch Stress Method 18
Figure 5. Finite Element Models for Global Structural Behaviors 21
Figure 6. Saddle Connections Simulated Using 3D Solid Elements in Models Created for Evaluating Global Behaviors of Overhead Truss Sign Structures 22
Figure 7. Fatigue Loads Placement on 60 ft Sign Structure 23
Figure 8. Designations of Saddle Connections 24
Figure 9. Models Created for Structural Hot Spot Stress Analysis 29
Figure 10. Mesh of Saddle Connections in Models for Structural Hot-Spot Analysis 30
Figure 11. Node Paths along Weld Toes for Extracting Structural Hot Spot Stresses 31
Figure 12. Fatigue Resistance Curve for Aluminum for Structural Hot-Spot Analysis 32
Figure 13. Contour Plots of Maximum Principal Stress of Saddle Connections of 137 ft Sign Structure . 32
Figure 14. Maximum Principal Stress Range along Node Path of Stiffener-to-Pipe Weld of Bottom Saddle Connection in 137 ft Span Sign Structure 33
Figure 15. Maximum Principal Stress Range along Node Path of Pipe-to-Plate Weld of Bottom Saddle Connection in 137 ft Span Sign Structures 33
Figure 16. Minimum Principal Stress Range along Node Path of Pipe-to-Plate Weld of Bottom Saddle Connection in 137 ft Span Sign Structures 34
Figure 17. Peak Structural Hot Spot Stresses with Fatigue Resistance Curves 35
Figure 18. Models Created for Effective Notch Stress Method 37
Figure 19. Stiffener-to-Support Frame Detail in Bottom Saddle Connection 38
Figure 20. Mesh of Welded Stiffener to Support Frame Pipe Detail in Bottom Saddle Connection 38
Figure 21. Welded Support Frame Pipe to Support Plate Detail of Bottom Saddle Connection 39
Figure 22. Welded Support Frame Pipe to Support Plate Detail of Top Saddle Connection 40
Figure 23. Contour Plots of Welded Detail Cross-Sections where Peak Maximum Principal Stresses Locate in Effective Notch Stress Analysis 41
Figure 24. Effective Notch Stress vs. Resistance Curves of AASHTO and IIW 42
Figure 25. 60 ft and 137 ft Overhead Truss Sign Structures Created Using Beam Elements 44
Figure 26. Loads Applied on Overhead Truss Sign Structure for Extreme Loading Analysis 45
Figure 27. Bottom and Top Saddle Connection Models for Extreme Loading Analyses 46

Figure 28. Loads Applied on Saddle Connections for Extreme Loading Analysis 46
Figure 29. 60 ft Span Sign Structure at Termination of Analysis 48
Figure 30. 137 ft Span Sign Structure at Termination of Analysis 49
Figure 31. Load-Displacement of Bottom Saddle Connection under Horizontally Applied Load 50
Figure 32. Load-Displacement of Bottom Saddle Connection under Upwardly Applied Load 50
Figure 33. Load-Displacement of Bottom Saddle Connection under Downwardly Applied Load..... 51
Figure 34. Load-Displacement of Bottom Saddle Connection under Axially Applied Load 51
Figure 35. Load-Displacement of Top Saddle Connection under Horizontally Applied Load..... 52
Figure 36. Load-Displacement of Top Saddle Connection under Upwardly Applied Load..... 53
Figure 37. Load-Displacement of Top Saddle Connection under Downwardly Applied Load 53
Figure 38. Load-Displacement of Top Saddle Connection under Axially Applied Load..... 54

List of Tables

Table 1. Loads Applied in Model of 60 ft Overhead Truss Sign Structure 24
Table 2. Peak Load Components at the Ends of 60 ft Truss 25
Table 3. Peak Load Components at the Ends of 83 ft Truss 26
Table 4. Peak Load Components at the Ends of 110 ft Truss 26
Table 5. Peak Load Components at the Ends of 137 ft Truss 27
Table 6. Peak Structural Hot Spot Stresses of Top Saddle Connections 34
Table 7. Peak Structural Hot Spot Stresses of Bottom Saddle Connections 34
Table 8. Section Forces of 60 ft Span Sign Structure at Termination of Analysis 48
Table 9. Section Forces of 137 ft Span Sign Structure at Termination of Analysis 49
Table 10. Summary of Loads at Starts of Localized Yielding and Global Plastic Behavior of Bottom Saddle Connection 51
Table 11. Summary of Loads at Starts of Localized Yielding and Global Plastic Behavior of Top Saddle Connection 54
Table 12. Interaction Equation Calculation of Section Forces at Connections at Analysis Termination of Overall Structures 55

1. Background

1.1 Introduction of Saddle Connection

A bridge-type overhead truss sign structure (OHTSS) is comprised of a 3D truss and two support-frames at each end. This type of sign structure is widely used on highways across the United States. Many commonly-used sign structure details can be found in Chapter 11 of the AASHTO Specifications for Structural Supports for Highway Signs, Luminaires, and Traffic Signals (AASHTO 2009). However, many state DOTs use their own types of connections that are not documented in the specification. The Kansas DOT has traditionally used a coupler-type joint in aluminum OHTSS to connect support-frame poles and truss chords, as shown in Figure 1. The interior two half-couplers are riveted together in a fabricating shop. During construction, the exterior half-couplers are bolted onto the riveted interior pieces to hold the support-frame pole and the truss chord in place. The coupler connection was originally designed in 1970s, and there are approximately 450 aluminum OHTSS using this type of connection over active highways in Kansas. However, there are two major disadvantages of the coupler connection. First, it is un-inspectable detail, since the two interior half-couplers are connected by a single rivet and the rivet is not visible after the connection is made. Second, assembling the coupler connection is a difficult task since the truss needs to be otherwise supported while workers install the couplers.

(a) Coupling Assembly (b) Interior Two Half-Couplers Riveted Together

Figure 1. Coupler Connection Traditionally Used on Aluminum Overhead Truss Sign Structures in Kansas

In 2015, Kansas DOT developed a new type of connection, the *saddle connection*, to use in new construction instead of the coupler connection that had been used for decades in aluminum

OHTSS. As shown in Figure 2, the saddle connection consists of a base plate, a saddle, stiffeners used to strengthen the connection between the base plate and the saddle, and one or two half-couplers (identical to those used in the coupler connections) for the bottom and top chord respectively. The truss chord is fixed onto the saddle through the half-couplers, which are bolted to the base plate. The saddle connections are more inspectable than the coupler-type connections once erected, and also make the construction process more straight-forward. The truss is able to rest securely on the saddles while workers fasten the half-couplers to the base plate.

(a) Connection for Bottom Chord (b) Connection for Top Chord

Figure 2. Saddle-Type Connections for Aluminum Overhead Truss Sign Structures

The primary load on sign structures are wind loads; therefore, it is essential to understand fatigue behavior of the connection. Bridge-type overhead sign structures are generally considered to be less sensitive to fatigue damage than cantilevered sign structures, but are not immune to fatigue damage. Kacin, et al. (2010) presented an investigation aimed at predicting the fatigue life of connections in OHTSS. The connections evaluated in their study were all found to perform within the infinite fatigue limit range. Nonetheless, fatigue at connection details in OHTSS has remained a topic of concern. NCHRP Project 17-10(2) reported a survey that indicated 8 out of 25 responding state DOTs reported fatigue-related problems associated with OHTSS (Fouad, et al. 2003). Foutch, et al. (2006) presented several failures at web diagonal strut-to-chord connections in aluminum OHTSS in a report to the Illinois DOT. Fam et al. (2006) presented a retrofit project for a K-shape diagonal strut-to-chord connection in aluminum OHTSS, and indicated that a large number of these structures suffer from fatigue cracking. Moreover, aluminum structures can be more sensitive to vibration problems due to their light weight, although steel overhead sign

structures are considered to rarely have this issue (Fouad, et al. 2003). Rice et al. (2012) indicated that overhead truss sign structures need to be evaluated for fatigue regardless of which AASHTO specifications or more advanced approaches are used.

The AASHTO Specifications for Structural Supports for Highway Signs, Luminaires, and Traffic Signals (AASHTO 2009) identifies four types of wind loads to be considered in fatigue design: galloping, natural wind, vortex shedding, and truck-induced gusts. For bridge-type OHTSS, only natural wind and truck-induced gusts need to be considered. Truck-induced gusts are recognized to induce smaller response than natural wind in OHTSS (Dexter and Ricker 2002). In an effort to validate the fatigue design wind loads presented by Yang et al. (2020), the suggested fatigue design load for truck-induced wind gusts is smaller than what is calculated according to AASHTO (2009). Dexter and Ricker (2002) also indicated that the design load for truck-induced gusts may be significantly overestimated. AASHTO (2009) indicates that truck-induced gusts should only be considered for OHTSS when required by the owner. The equations for determining the fatigue load of natural wind gusts and truck-induced gust in AASHTO (2009) are given in (Equation 1 and (Equation 2.

Natural Wind Gust

$$P_{NW} = 5.2 C_d I_F \quad \textbf{(Equation 1)}$$

Truck-Induced Gust

$$P_{TG} = 18.8 C_d I_F \quad \textbf{(Equation 2)}$$

Where,

C_d = Drag Coefficient

I_F = Fatigue Importance Factor

According to AASHTO (2009), natural wind gust loading is to be applied in the horizontal direction to the exposed area of all members, and truck-induced gust loading shall be applied in the vertical direction along any 12-ft length, excluding any portion not located directly above a traffic lane.

Because the number of cycles and the magnitude of stresses induced by wind loads are highly variable, designing a sign structure for finite fatigue life is not a practical approach. Therefore, AASHTO (2009) requires all sign structures to be designed for infinite fatigue life. For

steel structures, this means the stress range calculated using fatigue loads should be less than the constant amplitude fatigue threshold (CAFT) of the resistance curve. Structural details made of aluminum are usually considered to have no clear CAFT, but aluminum overhead sign structures are used in many states. For aluminum details, AASHTO (2009) requires designers to use the resistance curve for steel and divide it by 2.6.

As the saddle detail is a newly-developed connection, the Kansas DOT requires information about its mechanical performance. A research investigation is needed to characterize the structural performance that can be expected of the saddle connection, particularly regarding its fatigue susceptibility.

1.2 Fatigue Analysis Methods Using Finite Element Analysis

Finite element methods have been widely used in structural analysis, including investigations focused on characterizing fatigue performance. Three major fatigue analysis methods using finite element analysis include: nominal stress method, Hot Spot Stress (HSS) method, and the effective notch stress method. These are described briefly in the following sections to orient the reader.

1.2.1 Nominal Stress Method

The nominal stress approach to fatigue analysis relies on computation of nominal stresses for the detail in question, and comparison with established fatigue resistance curves (S-N curves) specific to that detail. The nominal stresses are calculated using design fatigue loads and nominal sectional areas. The effect of concentrated local stresses caused by geometric effects is not directly considered in the nominal stress calculation, but is inherently accounted for in the resistance curve (S-N curve), which is determined experimentally. The nominal stress method is the most traditional and widely-used approach for fatigue analysis and design. However, the nominal stress method has two major drawbacks. First, it does not explicitly account for variations in geometries within each detail category – in other words, each fatigue category is intended to capture a broad range of details. Second, some structural connection details are quite complicated, such that determining a nominal stress is not practical, and in some cases, impossible (Niemi et al. 2018).

1.2.2 Structural Hot Spot Stress Method

In contrast to the nominal stress method, the Structural Hot-Spot Stress (HSS) method takes into account the actual geometries of a detail. The Structural Hot Spot Stress is intended to capture the magnitude of stress at the anticipated crack initiation site. It can be measured experimentally or obtained through finite element analysis. The Structural Hot Spot Stress directly captures the effects of stress concentration from local geometries, but not the effect of the notch at the weld toe. The latter induces a nonlinear stress peak at the weld toe. The notch effect is considered in the experimentally-determined hot spot S-N curve.

Because the Hot-Spot Stress is extracted at the surface of the connected parts near the weld toe, the method is applicable for analyzing weld toe cracking, but it is not intended to quantify weld root cracking or cracks that might initiate at the surface of a weld (Hobbacher 2008). Other methods have been developed that use local nominal stress or structural stress derived from the stress distribution in the weld to analyze weld root cracking (Fricke 2012).

As element size at the weld toe approaches zero, computed stress at the weld toe will approach infinity – presenting a practical problem for accurate numerical predictions for fatigue performance. To obtain the Structural Hot-Spot Stress, surface stress extrapolation is commonly used. The Structural Hot Spot Stress can be obtained by linear extrapolating stress values back to the weld toe, extracting stress at a distance 0.4t or 1.0t away from the weld toe (t is the thickness of the plate) (Niemi et al. 2018). Stresses at a distance equal to 0.5t and 1.5t can also be adopted (Niemi et al. 2018; DNV 2011). Other than linear extrapolation, stress can also be directly extracted from the model a certain distance away from weld toe, for example, at distance 0.5t away from the weld toe (Niemi et al. 2018; DNV 2011). Because the stress extracted at a distance 0.5t away from the weld toe will be smaller than stresses approximated at the weld toe using a two-point extrapolation procedure, the directly-extracted stress magnitude is increased by a factor of 1.12 in the Det Norske Veritas (DNV) fatigue specifications (2011) or is used with a fatigue resistance curve that is one class/category lower (Niemi et al. 2018). Note that Niemi et al. (2018) recommends IIW FAT 90 to be used as the resistance curve for steel and one class lower than that

is FAT 80. The difference between these two fatigue classes corresponds to a decrease in resistance by a factor of 1.125, similar to that contained in the DNV recommendation.

For tubular joints, a more commonly-adopted method is to extract stress at a distance $0.1\sqrt{rt}$ away from the weld toe, where *r* is the radius of the pipe and *t* is the pipe thickness (DNV 2011; AASHTO 2009). This is the Structural Hot Spot Stress method that is described in the AASHTO Specifications for Structural Supports for Highway Signs, Luminaires, and Traffic Signals (AASHTO 2009). Similar methods using linear extrapolation also exist (DNV 2011).

Niemi et al. (2018) defined Structural Hot Spot Stress as 1) the larger principal stress if its direction is between 30° to 90° of the weld toe; 2) if the direction of the larger principle stress is outside the aforementioned limit, the larger of the stress component perpendicular to the weld toe and the minimum principal stress should be used. AASHTO (2009), however, only requires the maximum (tensile) principal stress to be analyzed. Niemi's definition sounds more rational since the heat-affected zone (HAZ) in front of a weld toe may very likely be in a state of high tensile residual stress, thus compressive stress flutations may still contribute to fatigue cracking. Moreover, the minimum (compressive) principal stress may be the component that is perpendicular to the weld toe and with a larger absolute value. Therefore, only analyzing maximum (tensile) stresses may result in obtaining unconservative conclusions. In the DNV provisions for tubular connections, the stress at a distance $0.1\sqrt{rt}$ away from the weld toe can be direcly used as the Structural Hot Spot Stress. For plate connections, the effective Hot Spot Stress is defined as the largest among $\sqrt{\Delta\sigma_{\perp}{}^2 + 0.81\Delta\tau_{\parallel}{}^2}$ (where $\sigma_{\perp}$ is the stress perpendicular to the weld toe and $\tau_{\parallel}$ is the stress parallel to the weld toe), factored maximum principal stress, and minimum principal stress.

For the resistance curve, fatigue guidance from the International Institute of Welding (IIW) (Hobbacher 2008) classifies different details and recommends use of either the FAT 100 or FAT 90 curves for steel and FAT 40 or FAT 36 for aluminum. Guidance in DNV (2011) indicates that its Category D curve should be used as the resistance S-N curve for Hot Spot Stress analysis. AASHTO (2009) requires the Hot Spot Stress to be compared with its fatigue Category C-curve. The DNV D-curve, IIW FAT 90, and AASHTO's C-curve are the same in the finite life region. The AASHTO Category C curve, DNV Category D curve, and IIW FAT 90 curve (for high-cycle applications) are plotted together in Figure 3. For aluminum details, AASHTO (2009) recommends

designers use the resistance curve for steel and divide by 2.6. IIW (Hobbacher 2008) recommends FAT 36 for aluminum. Note that FAT 36 is the same as Fat 90 divided by 2.5 (FAT 90 is the resistance curve recommended for steel). DNV (2011) does not give a recommendation for aluminum.

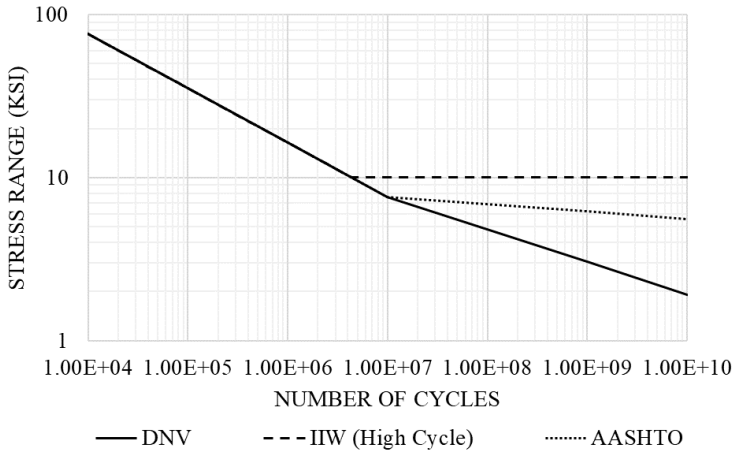

Figure 3. Fatigue Resistance S-N Curve of Steel Details for Hot Spot Stress Analysis

AASHTO (2009) indicates in its Appendix D that the Hot Spot Stress method is only applicable when evaluating *finite* life of the connection – for example, when assessing remaining fatigue life. For evaluating *infinite* fatigue life, an approach called effective notch stress method should be used. This is a difference from fatigue specifications published by IIW (Hobbacher 2008, Niemi et. al 2018, and Fricke 2010) and DNV (2011).

When developing finite element models for use with the Hot Spot Stress method, linear elastic material properties are usually adopted. Niemi et al. (2018) and DNV (2011) recommend that researchers use 8-node shell elements or 20-node solid elements with reduced integration. AASHTO (2009) requires the 20-node solid element to be used, and mesh size of $t \times t$ to be used for at least 3 element rows in front of the weld toe. At least two elements must be used in the through-thickness direction. A maximum element aspect ratio of 1:4 is specified, and the elements should have corner angles between 30° and 150°. IIW (Niemi et al. 2018) indicates that for a Type A weld toe (a weld toe on the surface of the plate), a relatively fine model should have elements smaller than the lesser of $0.4t \times t$ and $0.4t \times w/2$, where w is the longitudinal attachment thickness plus two times the weld leg length. For a fine model, the Hot Spot Stress should be extrapolated at the weld toe using the stresses at $0.4t$ and $1.0t$, and when using the single point stress method, the

fine mesh model is recommended. For a relatively coarse model, the elements should be $t \times t$ and not larger than $t \times w$. Stresses used for Hot Spot Stress extrapolation should be obtained at $0.5t$ and $1.0t$ for the coarse model. Niemi et al. (2018) indicates that when using the 20-node solid element, only one layer of elements is required through the thickness of the plate. DNV (2011) requires that the first two or three elements in front of weld toe in a tubular joint should be chosen as $t \times t$. The breadth of the element should be smaller than the thickness of the attached plate plus two times the weld leg length, and the length of the element should not exceed $2t$. DNV (2011) recommends elements to have corner angles between 60° and 120° and aspect ratios less than 5.

When developing finite element models, the size of the model should be large enough that the adopted boundary conditions do not significantly affect the results. Sub-modeling and sub-structurings technique can be used to create such models (Fricke 2010). In the sub-modeling method, a detailed model of the part of the structure of interest is created. Loads or displacements to be applied on the sub-model can be obtained by analyzing a coarser model of the overall structure. It is important that the sub-model has the same stiffness as the detail to be analyzed in the overall structure (Fricke 2010). Otherwise, incorrect local stresses will be obtained, depending on the difference between the stiffnesses and the load or displacement methods used. In the sub-structure technique, the detailed local model is inserted into the overall model as a sub-structure. This avoid the stiffness problem but care still need to make sure the connection to the overall structure at the boundary of the sub-structure does not significantly affect the results (Fricke 2010).

1.2.3 Effective Notch Stress Method

When using the Effective Notch Stress method, linear-elastic material properties are assumed. An effective weld is adopted to account for the variation of the weld shapes and non-linear material behavior at the weld notch (Hobbacher 2008). An effective notch root radius of 1 mm (0.04 inch) has been widely used (Fricke 2010; DNV 2011; AASHTO 2009). The Effective Notch Stress is the total stress at the root of a notch. The method can be used to assess fatigue cracking occuring at both a weld toe and a weld root.

For a fillet weld, the corner formed by the plate surface and the weld toe is modeled as being rounded with a specified radius of 1 mm (0.04 inch). For a weld root, a keyhole or a U-

shaped hole should be be created (Fricke 2010). It needs to be noted that a U-shaped hole may reduce the stress concentration as compared to a key-hole notch, and therefore, may yield unconservative results (Fricke 2010).

The IIW (Fricke 2010) indicates that for proportional loading, the first (maximum) principal stress range acting approximately perpendicular to the weld line should be used as the effective notch stress if the second principal stress has the same sign. Equivalent von-Mises stress can be used with a reduced-resistance S-N curve. An interaction formula with normal and shear stress can also be adopted. AASHTO (2009) and DNV (2011) state that the maximum tensile surface stress in the notch should be used as the effective notch stress.

When constructing the finite element models, AASHTO (2009) requires that 20-node solid isoperimetric element with reduced integration to be used. And at least eight elements should be used along the rounded notch perimeter at a weld toe (a quarter of a circle). The maximum aspect ratio should be limited to 1:4, and the element should have corner angles between 30° - 150°. DNV (2011) indicates that if the 20-node solid element is used, at least four elements should be used along a quarter of the circle circumference. The first three elements adjacent to the notch should be made with regular shapes without any element size transition. IIW (Fricke 2010) recommends at least three 20-node solid elements should be arranged along the rounded notch curve at the weld toe, which gives a maximum element size of 0.25 mm (0.01 in.) if a 1 mm (0.04 in.) notch radius is adopted (Fricke 2010).

The IIW (Fricke 2010) indicates that for weld toes, the effective notch stress should not be less than 1.6 times the Structural Hot Spot Stress.

As for the resistance curve, IIW (Fricke 2010) recommends FAT 160 to be used for steel and FAT 71 to be used for aluminum when maximum principal stresses are extracted. When von-Mises stresses are used, a reduction of one fatigue class is recommended. The standard form of the S-N curve in the DNV (2011) is expressed as $\log N = \log \bar{a} - m \log S$. For steel structures in air, the recommended resistance curve for $N \leq 10^7$ cycles has m = 3.0, $\log \bar{a}$ = 13.358; and for $N > 10^7$ cycles, m = 5.0, $\log \bar{a}$ = 17.596 (DNV 2011). DNV does not provide recommendations for aluminum structures. AASHTO (2009) indicates that the effective notch stress method should be used to evaluate infinite fatigue life. AASHTO (2009) requires the fatigue resistance to be

calculated as $(\Delta F)_l = \frac{1}{3.2}\left[-F_y + \sqrt{{F_y}^2 + 4{F_u}^2}\right]$, with F_y equal to the material yield strength and F_u equal to the ultimate tensile strength, both in ksi. The resistance curves determined according to DNV (2011), IIW (Fricke 2010) and AASHTO (2009) for steel are presented in Figure 4. The resistance shown here for AASHTO has been calculated assuming F_y = 50 ksi and F_u = 65 ksi. As shown in Figure 4, differences are evident in the fatigue resistance for effective notch stress method.

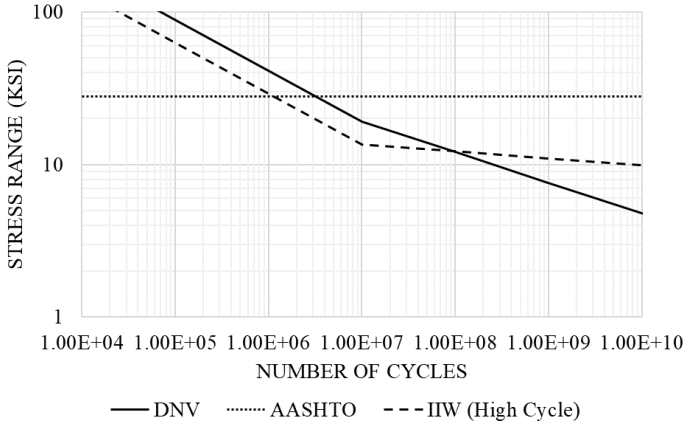

Figure 4. Fatigue Resistance S-N Curve of Steel Details for Effective Notch Stress Method

2. Objective and Scope

This study was aimed at evaluating the fatigue performance of the saddle connection using finite element analysis. The Hot-Spot Stress (HSS) and the Effective Notch Stress methods were applied to characterize fatigue demand and resistance. This study also considered the behavior of the connection and the structure under strength-level loading to evaluate ultimate strength performance.

The study consisted of four parts. The first part was aimed at determining the global behavior of OHTSS and identifying the location of critical connections under design fatigue loading. OHTSS having four span lengths, including 60 ft, 83 ft, 110 ft, and 137 ft, were created using the commercially-available finite element analysis software Abaqus v.2016. The framing of the sign structure was simulated using 3D beam elements, while the eight saddle connections were modeled using 3D solid elements. The location of critical connections was obtained by comparing peak section forces and moments at the ends of the truss beam elements.

The second part was focused on determining Hot Spot Stresses for the critical saddle connections. Detailed finite element models were created for saddle connections at each of the critical locations determined in the first part, using a sub-structure technique. The main body of the structure, created using 3D beam elements, was combined with one saddle connection assembly that was simulated using 3D solid elements and having detailed geometries and interactions. Welds were simulated as prismatic parts with a triangular cross-section and were tied to the members they connected. Hot Spot Stresses were extracted at node paths $0.1\sqrt{rt}$ away from the weld toes on pipes, and $0.5t$ away from weld toes on plates (r is the radius of the pipe, and t is the thickness). The peak Hot Spot Stresses were then compared with resistance curves as recommended in AASHTO, IIW, and DNV.

In the the third part of the study, three models were created to apply the effective notch stress method and to consider the performance of the saddle connection in the context of infinite fatigue life. Finite element models of the 137-ft span OHTSS used in the second part were modified for this analysis. The models included: 1) a model capturing the weld detail connecting the stiffener and the pipe in the bottom saddle connection; 2) a model capturing the weld connecting the support plate and the pipe in the bottom saddle connection; and 3) a model capturing the weld connecting the support plate and the pipe in the top saddle connection. Other than the weld detail evaluated in each model, other parts and interactions were simplified since the method requires very fine meshing demanding significant computational resources.

The fourth part of the study was focused on evaluating the behavior of the saddle connection and the structure under strength-level loading. This part included two series of analyses. The first included creating models of the overall structures for the 60-ft OHTSS and the 137-ft OHTSS, using 3D beam elements. The second included creating detailed models for the saddle connections using 3D solid elements. Elastic-perfectly plastic material properties were used for this portion of the research, so that ultimate limit states could be studied. These models were loaded until they reached computational limits, characterized by loss of stiffness due to material yielding.

3. Part One: Global Behavior of OHTSS and Locating Critical Connections

3.1 Model Introduction

The finite element models described in this section were created to study the global behavior of the structures and determine the governing (maximum design) demands for saddle connections used in the OHTSS to connect the truss and supports. As shown in Figure 5, OHTSS models of four span lengths, 60 ft, 83 ft, 110 ft, and 137 ft, were created using the commercially-available finite element analysis software, Abaqus v.2016. Each OHTSS model utilized 8.625-in. diameter truss chords with a thickness of 0.322 in., 10.75-in. diameter support-frame pipes with a thickness of 0.365 in., 0.625-in. thick support plates and stiffeners for top saddle connections, and 1.0-in. thick support plates and stiffeners for bottom saddle connections.

Linear-elastic material properties were defined for all parts in the models used to characterize global demands and localized fatigue performance. The pipes used in the overall truss and support structures in OHTSS are made of aluminum, and these were defined in the models to have a modulus of elasticity of 10,000 ksi and a Poisson's ratio of 0.35. The couplers are made of ductile cast iron, and were modeled with a modulus of elasticity of 24,000 ksi and Poisson's ratio of 0.275. Bolts were modeled as having a modulus of elasticity of 29,000 ksi and Poisson's ratio of 0.3. The main body of the OHTSS was simulated using two-node linear beam elements in space (B31) while the eight saddle connections, including segments of the chord pipe and support frame pipe, were created using eight-node 3D solid elements (C3D8R). The sign panels were created using linear four-node shear elements (S4R). The saddle connections were created using solid elements, and connected to the overall structure through kinematic coupling, which restrains the nodes on the cross-section of the solid element connection / truss chord sub-assembly to the rigid body movement of the node of the beam element truss chord.

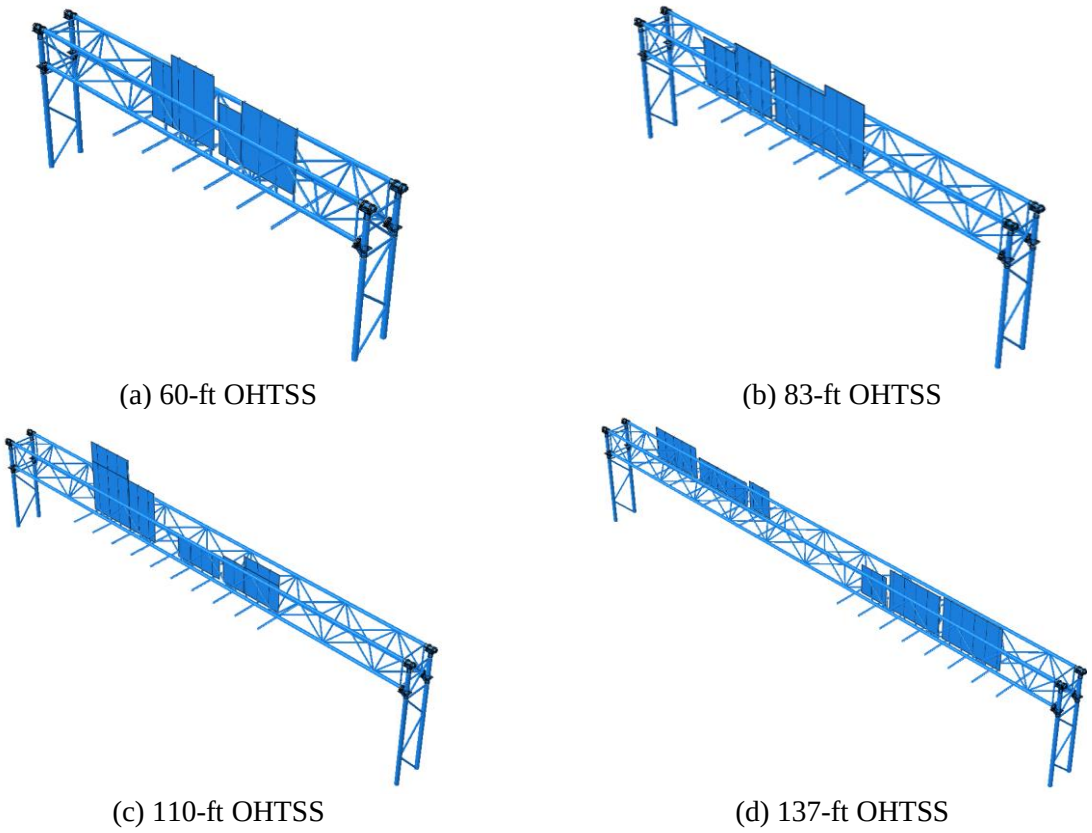

(a) 60-ft OHTSS (b) 83-ft OHTSS

(c) 110-ft OHTSS (d) 137-ft OHTSS

Figure 5. Finite Element Models for Global Structural Behaviors

The geometries of the connections are shown in Figure 6. The connections were assigned the actual geometries of each member, but geometries of welds were not simulated in these models, their influence instead being captured in this specific suite of models through tied constraints. The interactions between truss chords and the saddle connections were defined as hard contact with a friction coefficient of 1.1. Bolt heads were tied to the surfaces they attached to, and bolt shanks were in hard contact with bolt holes such that bolt pretension and bearing effects were simulated. The other contact interactions, including between welded parts and between couplers and chords were all simulated with tie constraints, which constrains degrees-of-freedom to the connected element. The geometries and interactions between members were simplified to reduce computational difficulties. Models with more detailed properties for the saddle connections were created in the second part and used to obtain Structural Hot Spot Stresses.

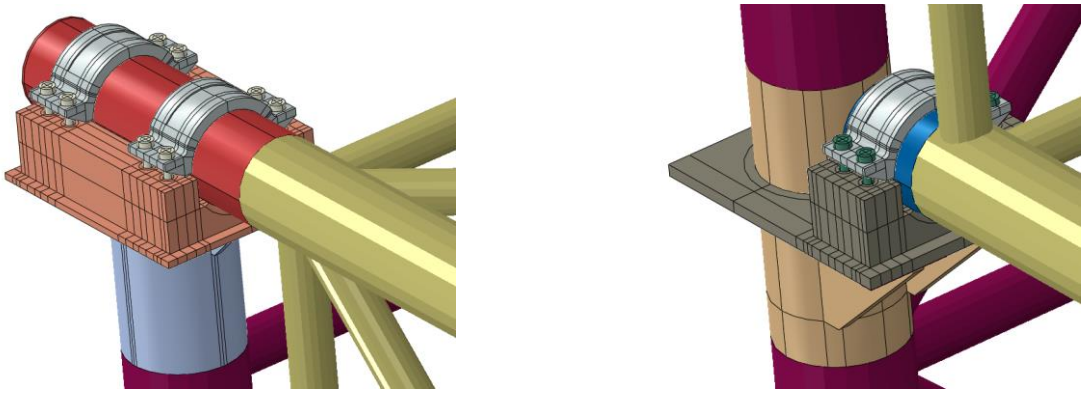

(a) Top Saddle Connection (b) Bottom Saddle Connection

Figure 6. Saddle Connections Simulated Using 3D Solid Elements in Models Created for Evaluating Global Behaviors of Overhead Truss Sign Structures

Fatigue loads were applied as static loads in Abaqus, including natural wind gusts and truck-induced gusts, and were calculated according to AASHTO (2009). Six loading modes were considered, including natural wind gusts applied at front, back, and side of the structure, and truck-induced gusts applied over a 12-ft horizontal projection at right, middle, and left of the truss, as shown in Figure 7. The end nodes of the support frames were fixed by restraining all degree-of-freedoms. A 39-kip bolt pretension force was applied on each bolt in a separate step before applying the fatigue loads.

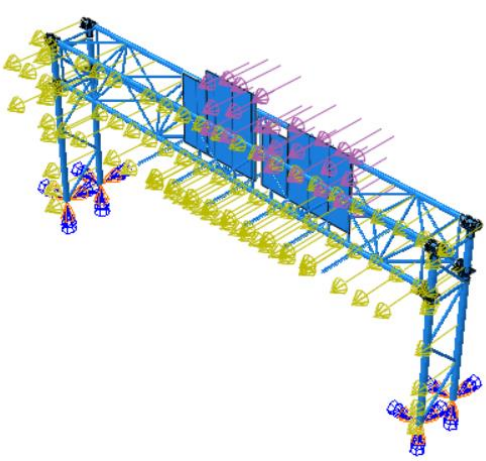

(a) Natural Wind from Back

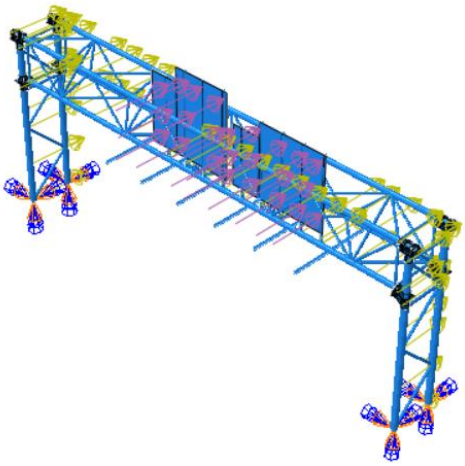

(b) Natural Wind from Front

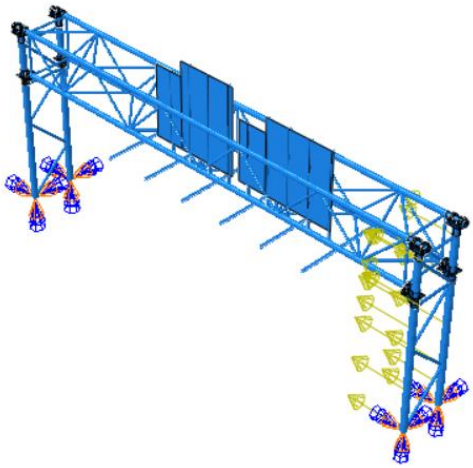

(c) Natural Wind from Side

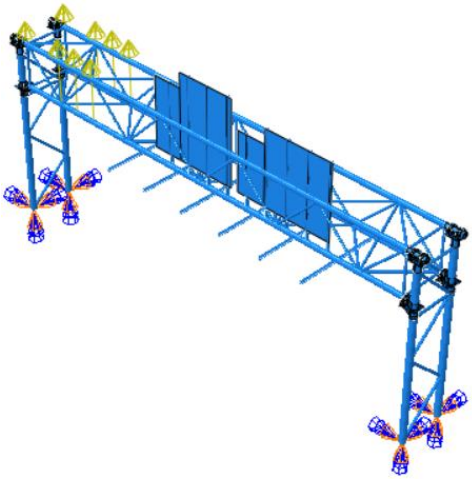

(d) Truck-Induced Gust at Left 12 ft

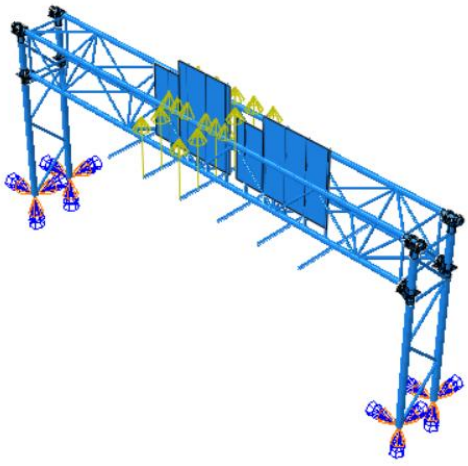

(e) Truck-Induced Gust at Middle 12 ft

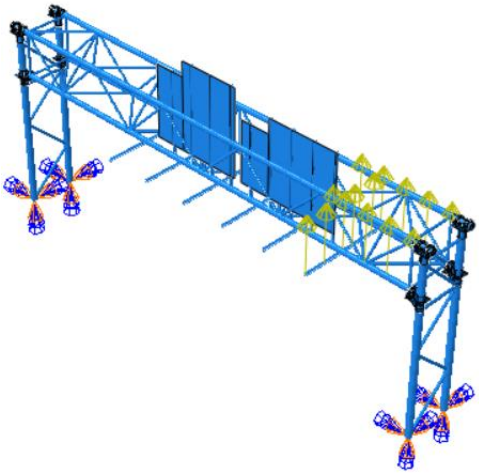

(f) Truck-Induced Gust at Right 12 ft

Figure 7. Fatigue Load Placements on 60-ft Sign Structure

The loads applied on the 60-ft sign structure are shown in Table 1. The loads applied on the other structures included in this study were slightly different, and are provided in Appendix A. A sample calculation for the 60-ft sign structure is provided in Appendix B.

Table 1. Loads Applied in 60-ft OHTSS Model

	NWB	NWF	NWS		TGL	TGM	TGR
Support Frame Pipe	0.00047 (kip/in)		Below Truss	0.00065 (kip/in)			
			Above Truss	0.0013 (kip/in)			
Truss Chord	0.00071 (kip/in)	0.00063 (kip/in)			0.0027 (kip/in)		
Sign Beam	0.00022 (kip/in)						
Sign 1	0.000043 (ksi)						
Sign 2	0.000041 (ksi)						
Walkway Beam					0.00078 (kip/in)		

3.2 Analysis Results

Designations assigned to the connections are shown in Figure 8. Peak section forces and moments are given in Table 2 to

Table 5. Critical connections were identified by comparing the peak section forces and moments at the end beam elements of the chords. The highlighted rows in Table 2 to

Table 5 show the selected critical connections.

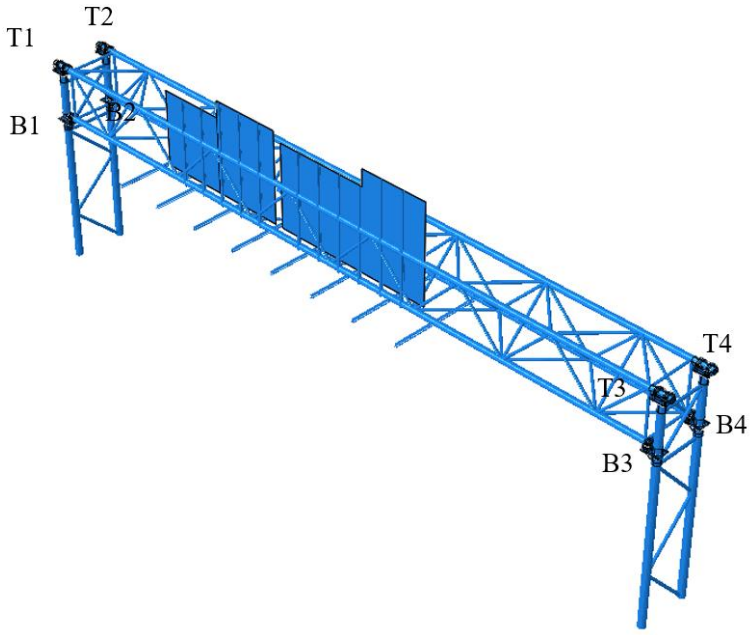

Figure 8. Designations for Saddle Connections

In the model of the 83-ft span OHTSS, connection T2 and B2 were identified as the critical connections, since their section forces were larger compared with those of other connections. However, identification of critical connections was not necessarily so obvious in all models included in the study. For example, in the 60-ft span model, connection B3 was found to possess the largest vertical shear, but connection B4 had the largest horizontal shear. Importantly, the peak loads in each connection were not found to be significantly different from each other. This is because the natural wind loads applied to the sign panel face almost always governed the results, and the structures are somewhat symmetric except for the position of the sign panel. Therefore, even though some judgement was sometimes necessitated in identifying the critical connection, the final Hot Spot Stress analysis result is not expected to have been significantly affected.

The connections identified as critical in each of the structures included in the study are as follows:

- 60-ft span – T3, B4;
- 83-ft span – T2, B2; and
- 110-ft span – T2, B2;
- 137-ft span – T4, B4.

Table 2. Peak Load Components at the Ends of the 60-ft Truss

(a) Bottom Connection

	Axial Load		Vertical Shear		Horizontal Shear		In-Plane Bending		Out-of-Plane Bending		Twisting	
	(kip)	% of Max	(kip)	% of Max	(kip)	% of Max	(Kip-in)	% of Max	(kip-in)	% of Max	(kip-in)	% of Max
B1	0.16	84	0.63	90	0.46	64	2.30	65	3.45	73	1.33	50
B2	0.12	61	0.59	84	0.61	84	3.18	90	3.43	73	2.22	84
B3	0.20	100	0.71	100	0.55	76	2.68	75	4.23	90	1.62	62
B4	0.15	76	0.66	93	0.73	100	3.55	100	4.72	100	2.64	100

(b) Top Connection

	Axial Load		Vertical Shear		Horizontal Shear		In-Plane Bending		Out-of-Plane Bending		Twisting	
	(kip)	% of Max	(kip)	% of Max	(kip)	% of Max	(kip-in)	% of Max	(kip-in)	% of Max	(kip-in)	% of Max
T1	0.12	75	0.47	90	0.35	81	2.36	86	3.11	70	1.24	88
T2	0.10	65	0.46	88	0.24	54	2.66	97	3.45	78	1.09	78
T3	0.16	100	0.52	100	0.44	100	2.45	89	4.43	100	1.41	100
T4	0.16	100	0.51	98	0.27	63	2.74	100	3.97	89	1.27	90

Table 3. Peak Load Components at the Ends of the 83-ft Truss

(a) Bottom Connection

	Axial Load		Vertical Shear		Horizontal Shear		In-Plane Bending		Out-of-Plane Bending		Twisting	
	(kip)	% of Max	(kip)	% of Max	(kip)	% of Max	(Kip-in)	% of Max	(kip-in)	% of Max	(kip-in)	% of Max
B1	0.37	100	0.69	82	0.56	90	4.99	100	5.21	88	1.32	66
B2	0.35	94	0.83	100	0.63	100	4.6	92	5.95	100	1.99	100
B3	0.27	73	0.5	60	0.49	77	3.24	65	4.71	79	1.21	61
B4	0.26	69	0.72	86	0.54	86	4.24	85	5.36	90	1.75	88

(b) Top Connection

	Axial Load		Vertical Shear		Horizontal Shear		In-Plane Bending		Out-of-Plane Bending		Twisting	
	(kip)	% of Max	(kip)	% of Max	(kip)	% of Max	(kip-in)	% of Max	(kip-in)	% of Max	(kip-in)	% of Max
T1	0.25	92	0.72	100	0.41	92	2.74	95	4.85	87	1.47	95
T2	0.24	87	0.66	92	0.45	100	2.62	91	5.56	100	1.55	100
T3	0.27	98	0.64	89	0.35	77	2.88	100	4.13	74	1.21	78
T4	0.27	100	0.43	60	0.39	87	2.63	91	4.94	89	1.37	88

Table 4. Peak Load Components at the Ends of the 110-ft Truss

(a) Bottom Connection

	Axial Load		Vertical Shear		Horizontal Shear		In-Plane Bending		Out-of-Plane Bending		Twisting	
	(kip)	% of Max	(kip)	% of Max	(kip)	% of Max	(Kip-in)	% of Max	(kip-in)	% of Max	(kip-in)	% of Max
B1	0.20	91	1.14	86	0.72	88	2.63	68	2.28	68	2.06	80
B2	0.20	90	1.33	100	0.82	100	3.85	100	3.23	96	2.58	100
B3	0.20	90	0.77	58	0.67	82	2.49	65	3.01	90	1.84	71
B4	0.22	100	0.91	68	0.70	85	3.47	90	3.36	100	2.36	91

(b) Top Connection

	Axial Load		Vertical Shear		Horizontal Shear		In-Plane Bending		Out-of-Plane Bending		Twisting	
	(kip)	% of Max	(kip)	% of Max	(kip)	% of Max	(kip-in)	% of Max	(kip-in)	% of Max	(kip-in)	% of Max
T1	0.11	77	0.74	100	0.40	84	2.82	100	3.24	73	1.28	84
T2	0.13	85	0.48	65	0.47	100	2.67	95	4.45	100	1.53	100
T3	0.13	89	0.60	82	0.33	71	2.50	89	3.45	77	1.41	92
T4	0.15	100	0.43	59	0.39	84	2.64	94	4.23	95	1.38	90

Table 5. Peak Load Components at the Ends of the 137-ft Truss

(a) Bottom Connection

	Axial Load		Vertical Shear		Horizontal Shear		In-Plane Bending		Out-of-Plane Bending		Twisting	
	(kip)	% of Max	(kip)	% of Max	(kip)	% of Max	(Kip-in)	% of Max	(kip-in)	% of Max	(kip-in)	% of Max
B1	0.24	95	0.90	70	0.87	84	2.42	70	2.20	60	2.70	76
B2	0.25	100	1.19	93	0.96	94	2.98	86	3.57	98	3.30	93
B3	0.23	94	1.09	85	0.97	94	2.24	65	2.63	72	2.80	79
B4	0.25	100	1.29	100	1.03	100	3.45	100	3.66	100	3.54	100

(b) Top Connection

	Axial Load		Vertical Shear		Horizontal Shear		In-Plane Bending		Out-of-Plane Bending		Twisting	
	(kip)	% of Max	(kip)	% of Max	(kip)	% of Max	(kip-in)	% of Max	(kip-in)	% of Max	(kip-in)	% of Max
T1	0.16	86	0.60	92	0.35	69	2.49	94	3.33	69	1.61	93
T2	0.17	91	0.43	66	0.44	88	2.54	96	4.55	95	1.52	87
T3	0.18	97	0.65	100	0.45	88	2.36	89	4.61	96	1.72	99
T4	0.18	100	0.43	65	0.51	100	2.66	100	4.81	100	1.74	100

The critical connections determined in this part of the study were then used in the models for Structural Hot Spot Stresses analysis and for Effective Notch Stress analysis.

4. Part Two: Structural Hot Spot Stresses (HSS) Analysis

4.1 Model Introduction

Detailed models were created for each critical connection as determined in Part One. This study adopted the sub-structure modeling technique for the construction of models for use with Structural Hot Spot Stresses analysis. The detailed connections were built as a sub-structure and embedded in the overall structure. It avoids the issue of different stiffness of a global model and a sub-model.

An example of the models created for Structural Hot Spot Stress analysis is shown in Figure 9. Similar as to the models described in Part One, linear-elastic material properties were defined for aluminum and ductile cast iron. The aluminum structural elements were assigned a modulus of elasticity of 10,000 ksi and a Poisson's ratio of 0.35. The couplers, which are made of ductile cast iron, were assigned a modulus of elasticity of 24,000 ksi and Poisson's ratio of 0.275. The main body of the structure created using linear 3D beam elements (B31) was combined with one detailed saddle connection simulated using the 20-node quadratic 3D solid elements (C3D20R). The detailed geometries and interactions were simulated as faithfully as possible, including the geometries of each weld and interactions between the threaded 'keepers' in each coupler and the aluminum chords. The fillet welds were simulated as bars or rings with triangular cross-sections

and were tied to surfaces they connected using tie constraints. A tie constraint constrains all degrees-of-freedom for one surface to that of the other surface being connected. The welds were all assigned a size of 0.5 in. Other interactions between the members welded together were not simulated, (realistically) assuming that the welds were the only load-transfer mechanism. All degrees-of-freedom of the nodes at the joints of the beam element truss and the beam element support frame were restrained to each other. The interactions between the chord and saddle and the chord and threaded 'keepers' were assigned hard contact properties with friction coefficients of 1.1 and 0.6, respectively. The saddle details created using solid elements and the overall structure were connected through kinematic coupling, which restrained the nodes on the cross-section of the solid element to the rigid body movement of the end node of the beam element.

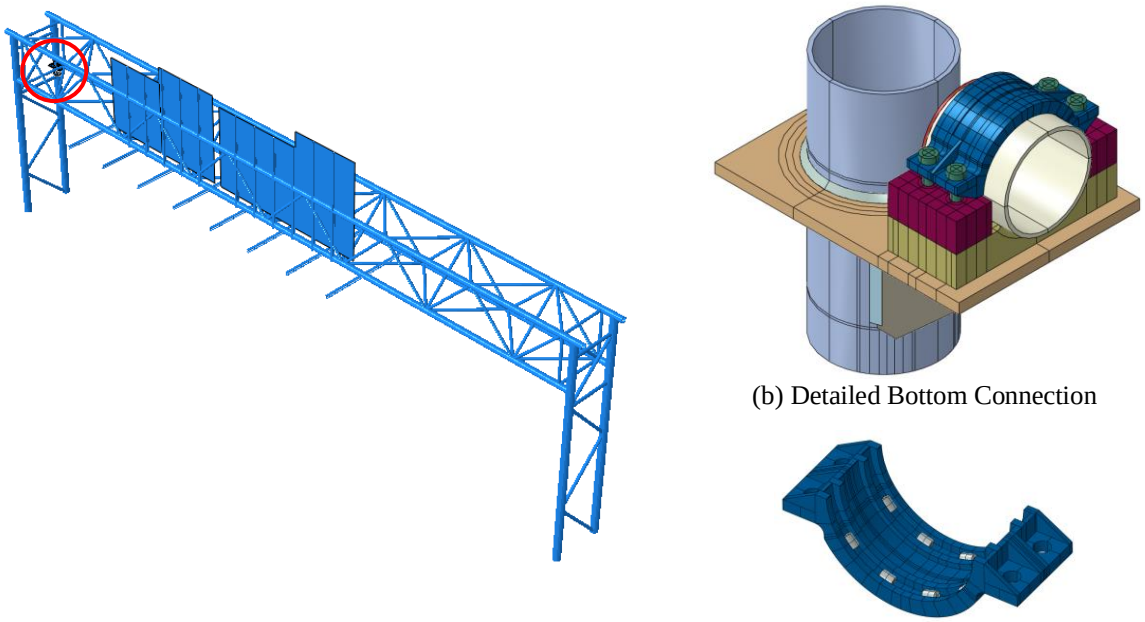

(a) Model with One Detailed Bottom Connection

(b) Detailed Bottom Connection

(c) Coupler with Keepers Simulated

Figure 9. Models Created for Structural Hot Spot Stress Analysis

The mesh used for the bottom and top saddle connections are shown in Figure 10. Regions close to the weld toes were assigned a mesh size of 0.14 in. on the support-frame pipes and 0.2 in. on the support plates and stiffeners. This density was maintained for at least the five element rows in front of the weld toes. There were two elements through-thickness in the support-frame pipes

and three elements through-thickness of support-plates and stiffeners. All elements close to a weld toe had corner angles between 30°-150° and aspect ratios smaller than 4:1. Regions further away from weld toes were assigned mesh sizes from 0.4 in. to 0.5 in.

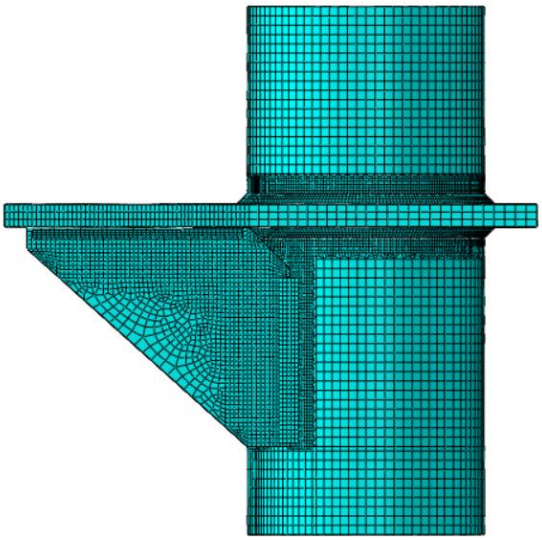

(a) Mesh at Support-Frame Pipe and Stiffeners in the Bottom Saddle Connection

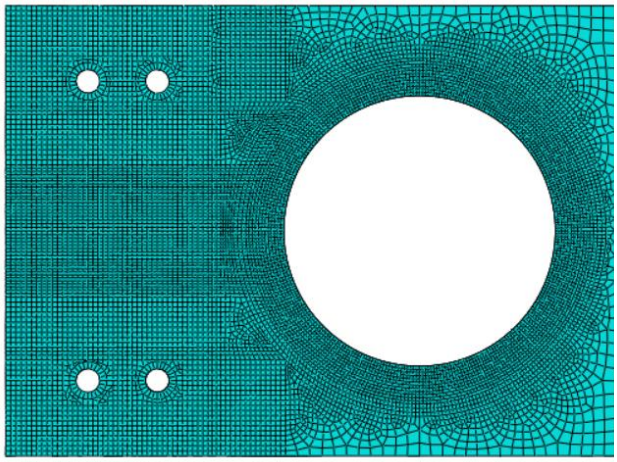

(b) Mesh at Support-Plate in the Bottom Saddle Connection

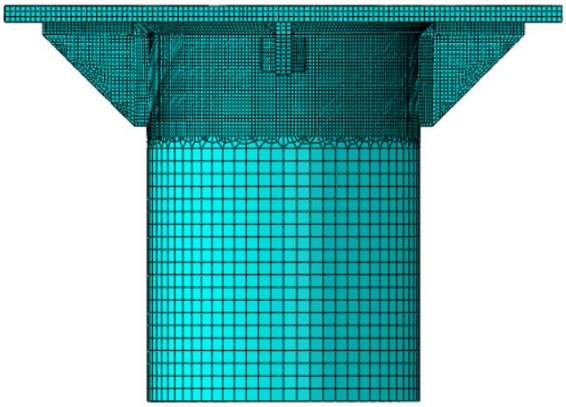

(c) Mesh at Support-Frame Pipe and Stiffeners in the Top Saddle Connection

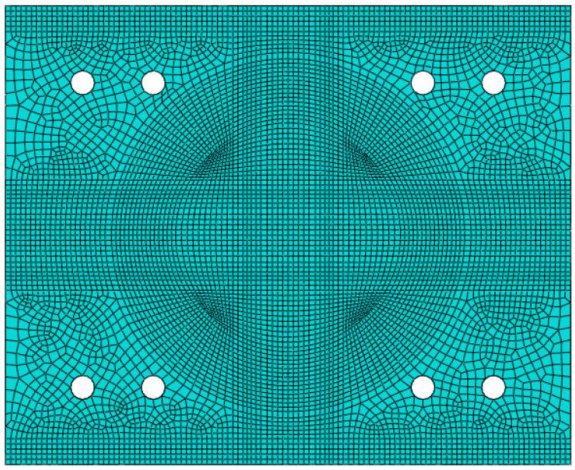

(d) Mesh at Support-Plate in the Top Saddle Connection

Figure 10. Mesh of Saddle Connections in Models for Structural Hot-Spot Analysis

This part of the study included HSS analyses for the four span length OHTSS subjected to the six loading modes introduced in Part One (Figure 5 and Figure 7). A 39-kip bolt pretension force was applied in a step *before* applying the fatigue loads.

Nodal paths were created along each weld toe to extract stresses; two nodal paths have been shown in Figure 11 as examples. In each model, 20 nodal paths were created for the bottom connection and 34 node paths for the top connection. Stresses were extracted at a distance of $0.1\sqrt{rt}$ (0.14 in.) away from weld toes on the support-frame pipes and $0.5t$ (0.5 in. and 0.3125 in. for bottom and top connections respectively) away from weld toes on the plates and stiffeners. The stresses obtained at $0.1\sqrt{rt}$ were directly used as Structural Hot Spot Stresses. The stresses obtained at $0.5t$ would be smaller than those obtained using extrapolation methods. Therefore, the stresses at $0.5t$ were increased by a factor of 1.12 as recommended in DNV (2012) and IIW (Niemi et al. 2018). The range of the larger principal stresses were output as the Structural Hot Spot Stresses. The stress range was calculated using the stress in each wind load step minus the stress in the bolt pretension step. As introduced the background section, IIW, AASHTO, and DNV have different requirement regarding which stress should be taken as the Structural Hot Spot Stress. However, it was considered conservative to use the larger principal stress.

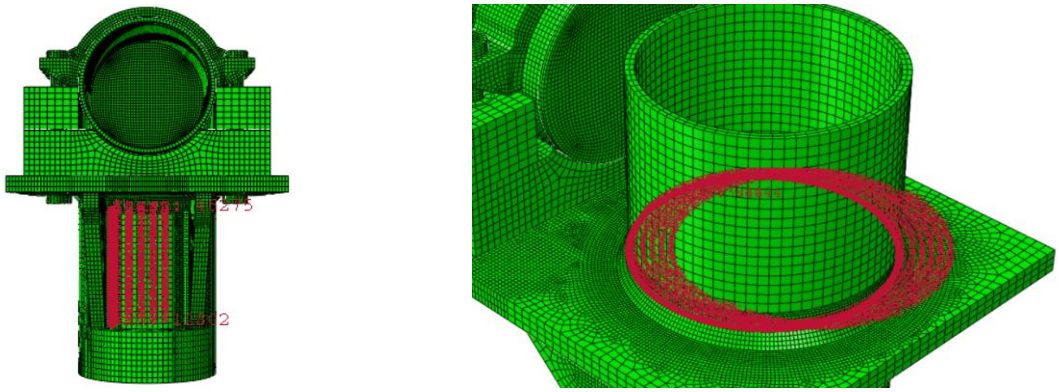

(a) Node Path along Weld Toe of the Vertical Weld Connecting Stiffener and Plate

(b) Node Path along Weld Toe of the Horizontal Weld Connecting Pipe and Plate

Figure 11. Node Paths along Weld Toes for Extracting Structural Hot Spot Stresses

The AASHTO Category C curve, divided by 2.6 to adjust for aluminum materials, and the IIW FAT 36 curve were used as the fatigue resistance curves. Although the DNV provides no recommendations for aluminum materials, a similar method to convert from steel to aluminum fatigue resistance curve can be adopted. In this study, the DNV Category D curve was divided by 2.6. The three curves are plotted in Figure 12.

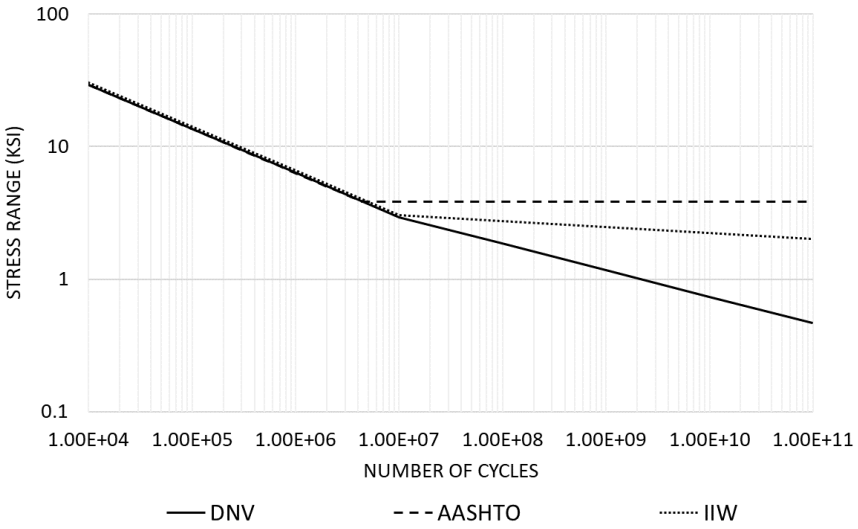

Figure 12. Fatigue Resistance Curve for Aluminum for Structural Hot-Spot Analysis

4.2 Analysis Results

Contour plots for maximum principal stress in the saddle connections in the 137-ft OHTSS are presented in Figure 13 as examples. The plots represent the total response occurring from natural wind blowing from the back of the sign panel, with bolt tensioning effects captured in the model. It is worth mentioning that the contour plots do not represent stress *fluctuations* under wind load since most of the stresses were actually induced by the bolt pretension. To determine *fatigue* demand, stresses arising from the wind load step minus stresses arising from the bolt load step were considered.

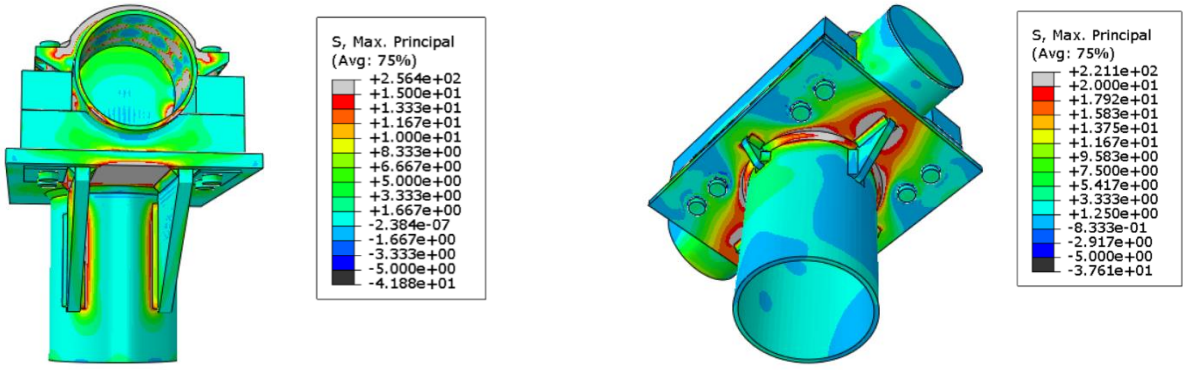

(a) Bottom Saddle Connection (ksi) (b) Top Saddle Connection (ksi)

Figure 13. Contour Plots of Maximum Principal Stress of Saddle Connections in the 137-ft OHTSS

Three plots of the principal stress range along the predefined node paths are provided as examples in Figure 14 to Figure 16. In almost all the analysis, the loading mode of natural wind blowing perpendicular to the sign panel produced the greatest stress ranges.

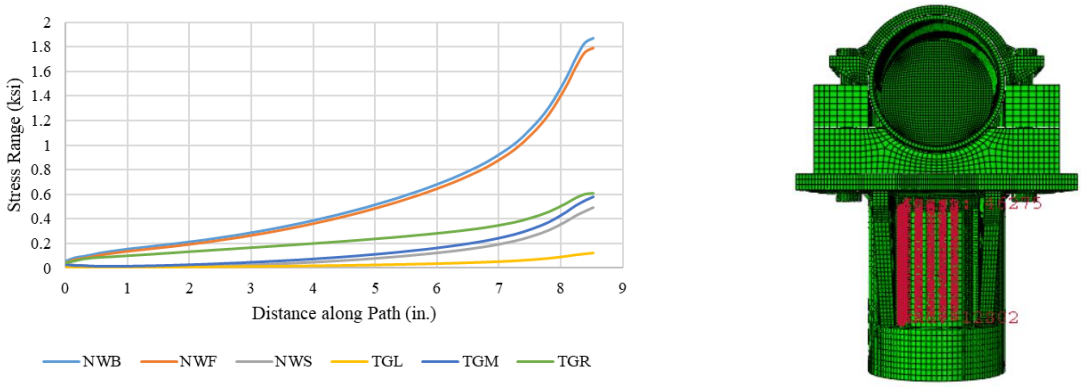

Figure 14. Maximum Principal Stress Range along Node Path of Stiffener-to-Pipe Weld of Bottom Saddle Connection in 137-ft OHTSS

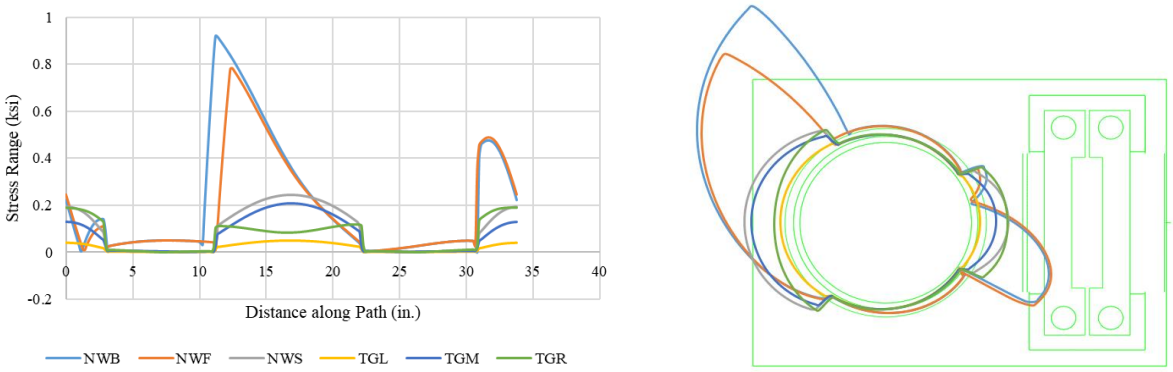

(a) Stress Range along Node Path (b) Stress Range Plotted around Weld

Figure 15. Maximum Principal Stress Range along Node Path of Pipe-to-Plate Weld of Bottom Saddle Connection in 137-ft OHTSS

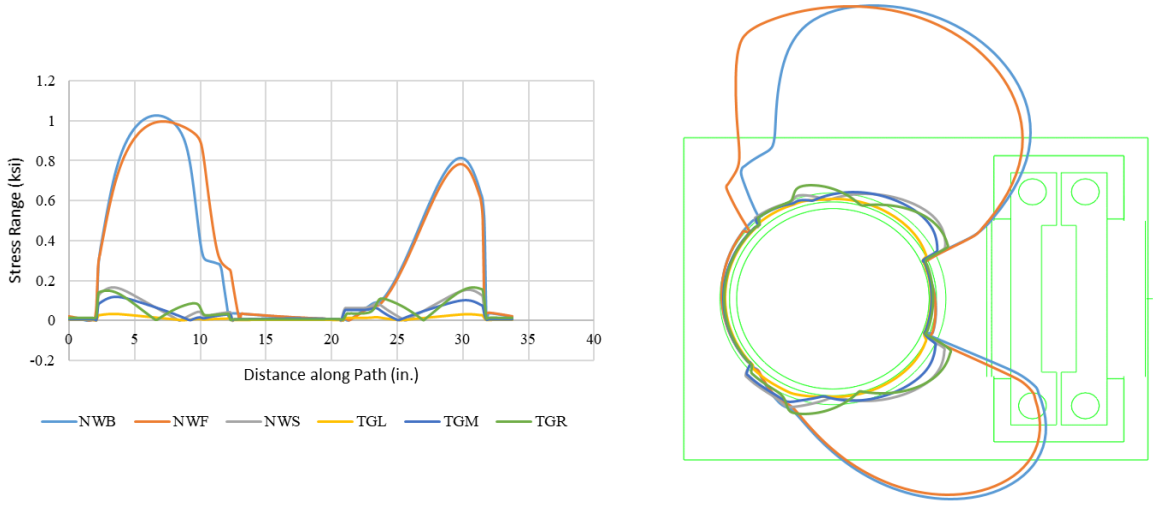

(a) Stress Range along Node Path (b) Stress Range Plotted around Weld

Figure 16. Minimum Principal Stress Range along Node Path of Pipe-to-Plate Weld of Bottom Saddle Connection in 137-ft OHTSS

The peak Structural Hot Spot Stresses extracted from each weld type have been summarized in Table 6 and Table 7. The Structural Hot Spot Stresses were taken as the larger between the maximum and the minimum principal stresses. The welds connecting the stiffeners to the support frame pipes in the bottom saddle connections exhibited the largest stresses, and therefore, were found to be the most susceptible details to fatigue. Moreover, the welds connecting the support plates to the support frame pipes in the bottom saddle connections also exhibited stresses considerably larger than other welds.

Table 6. Peak Structural Hot Spot Stresses for Top Saddle Connections

Location of Weld Toe		Structural Hot Spot Stress (ksi)			
		60 ft	83 ft	110 ft	137 ft
Pipe	Stiffener-Pipe Weld	0.54	0.62	0.64	0.57
	Plate-Pipe Weld	0.46	0.50	0.52	0.47
Plate	Pipe-Plate Weld	0.29	0.23	0.31	0.28
	Stiffener-Plate Weld	0.32	0.35	0.37	0.27
Stiffener	Plate-Stiffener Weld	0.20	0.17	0.22	0.19
	Pipe-Stiffener Weld	0.40	0.35	0.45	0.37

Table 7. Peak Structural Hot Spot Stresses for Bottom Saddle Connections

Location of Weld Toe		Structural Hot Spot Stress (ksi)			
		60 ft	83 ft	110 ft	137 ft
Pipe	Stiffener-Pipe Weld	0.82	1.31	1.93	1.87
	Plate-Pipe Weld	0.44	0.67	0.85	1.01

Plate	Pipe-Plate Weld	0.29	0.20	0.34	0.38
	Stiffener-Plate Weld	0.06	0.06	0.09	0.08
Stiffener	Plate-Stiffener Weld	0.10	0.13	0.19	0.20
	Pipe-Stiffener Weld	0.14	0.24	0.30	0.31

The peak Structural Hot Spot Stresses extracted from each model were then plotted with the DNV, AASHTO, and IIW resistance curves, as presented in Figure 17. The bottom saddle connections were found to have the larger stresses for all span lengths. The stresses were all found to fall below the constant fatigue threshold of AASHTO resistance curve. The largest stress identified was below the knee point of the DNV and IIW curves, and intersected the two curves at approximately 10^8 cycles and 10^{11} cycles. It is important to note that these values cannot be used to predict the remaining life of a structure because the loading applied in this study was AASHTO fatigue loading and the number of cycles and stresses that would occur under a realistic distribution of real winds were not determined. However, the findings from this HSS analysis do indicate that fatigue damage is not expected to occur in normal use.

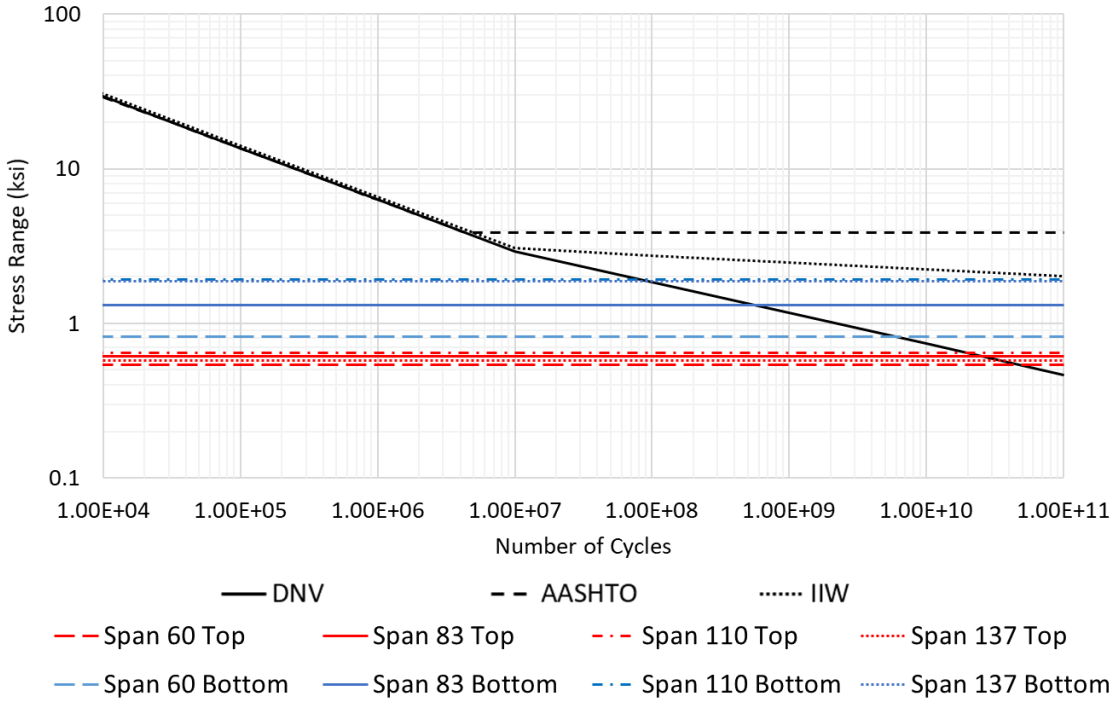

Figure 17. Peak Structural Hot Spot Stresses with Fatigue Resistance Curves

5. Part Three: Effective Notch Stresses Analysis

5.1 Model Introduction

As introduced previously, the Hot Spot Stress method cannot be used to predict the likelihood of fatigue cracking that may initiate at a weld root. Instead, the Effective Notch Stress method can be used for that purpose. This part of the study was also performed to fulfill the requirement of AASHTO (2009) that the Effective Notch Stress method should be used for infinite fatigue life analysis.

Three models were created for the 137-ft span structure. Each model was constructed for the purpose of analyzing one weld using the Effective Notch Stress method. These included: a model of the stiffener-to-support frame weld in the bottom saddle connection, a model of the support plate-to-support frame weld in the bottom saddle connection, and a model for the support plate-to-support frame weld in the top saddle connection. The AASHTO fatigue load for natural wind blowing from the back of the sign structure was applied.

The models in this part of the study were modified from those described in Part Two of this report. Linear-elastic material properties identical to those described in Parts One and Two of this report were adopted. Due to the computational demands associated with employing a very dense mesh, the models for the notch stress method were simplified as much as possible, as shown in Figure 18. Welds were removed from the model, other than the one being directly analyzed. The other connections were made using tie constraints. Bolts and couplers were removed from the models intended for use with the Effective Notch Stress method as superfluous to the goal of these analyses. Here, the chords were tied directly to the saddle, which was then tied to the support plate.

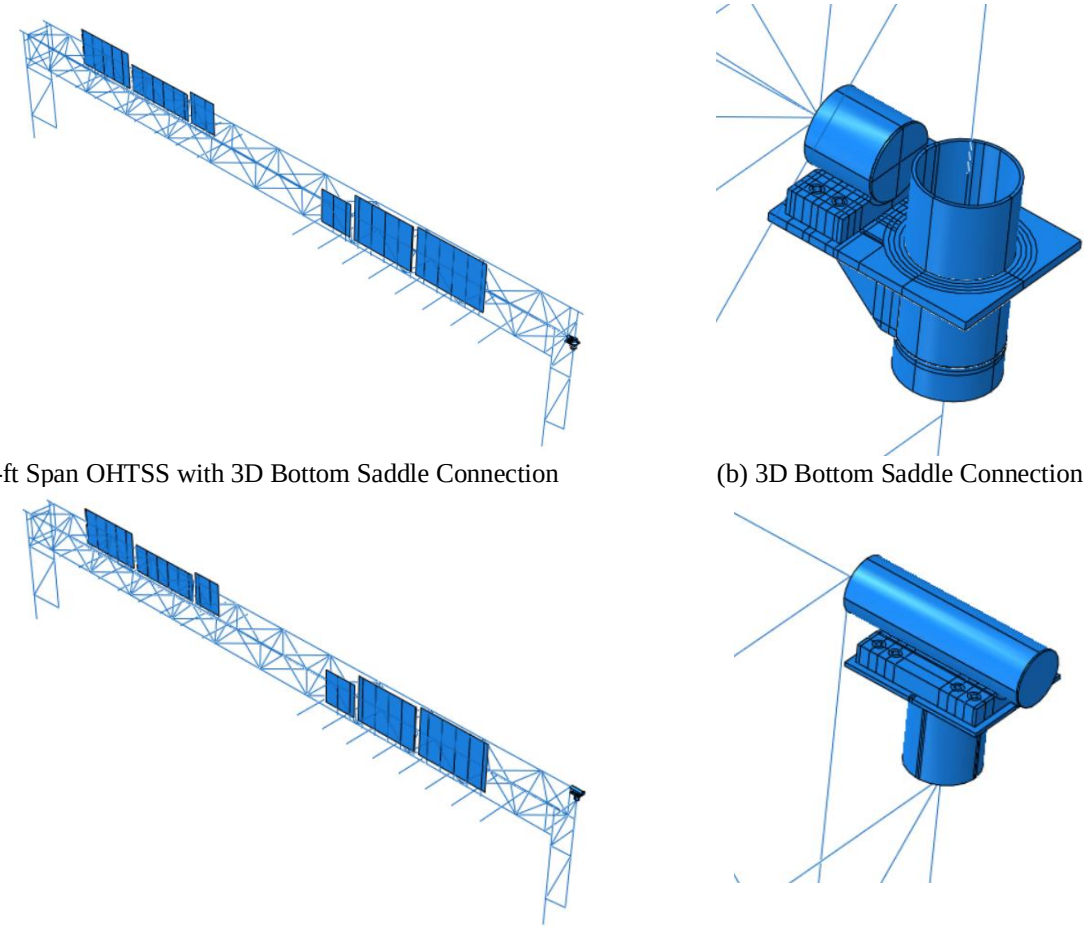

(a) 137-ft Span OHTSS with 3D Bottom Saddle Connection

(b) 3D Bottom Saddle Connection

(c) 137-ft Span OHTSS with 3D Top Saddle Connection

(d) 3D Top Saddle Connection

Figure 18. Models Created for Effective Notch Stress Method

In the model to be used for analyzing the stiffener-to-support frame weld in the bottom saddle connection, the welded members were created as four parts connected through tie constraints, as shown in Figure 19(a). Figure 19(b) shows a close-up of the portion of the overall detail labeled as "Part 1". Part 1 included the two welds connecting the stiffener to the pipe. The interior one was the weld being analyzed. Notches were created at the weld toes and the weld root that had a radius of 1 mm (0.04 inch). The notch at the weld root was created using the key-hole style, as shown in Figure 19(c).

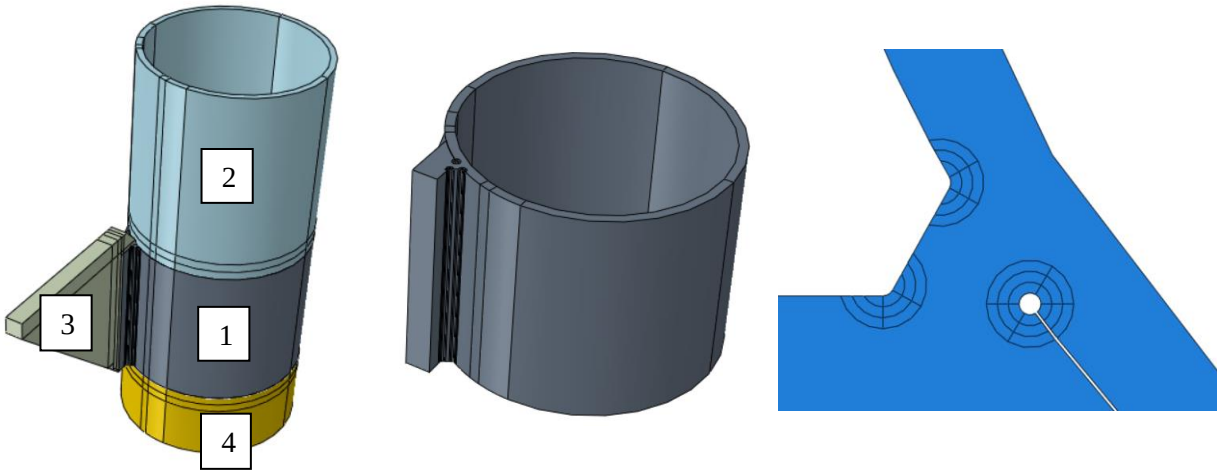

(a) Stiffener-to-Support Frame Detail

(b) Part One of Stiffener-to-Support Frame Detail

(c) Notches Created at Weld Root and Weld Toes

Figure 19. Stiffener-to-Support Frame Detail in Bottom Saddle Connection

The mesh structures used are shown in Figure 20. The mesh size at the notch was 0.01 in., and the mesh size in the direction perpendicular to the cross-section was 0.04 in. The elements were structured to have a regular shape near the notch. The regions further away from the weld being analyzed had a mesh size of 0.4 inch. The quadratic 20-node solid elements with reduced integration (C3D20R) were used in the part labeled as "Part 1" (Figure 19). Linear 8-node solid elements (C3D8R) were used in the other solid parts.

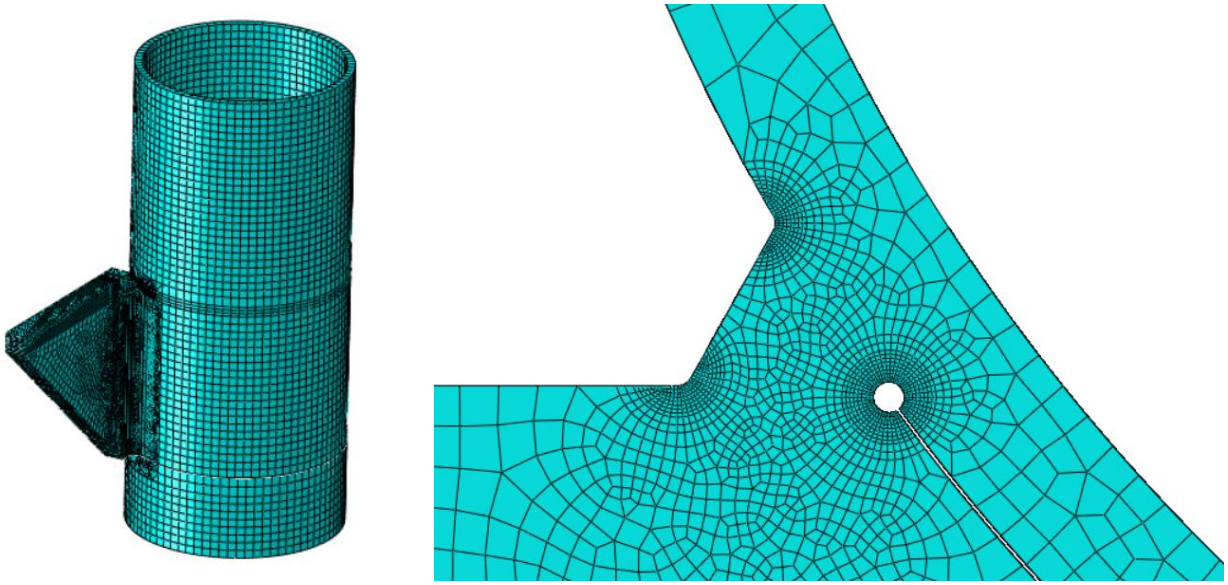

(a) Mesh of Welded Stiffener to Support Frame Pipe Detail

(b) Mesh at Cross-Section of Welded Stiffener to Support Frame Pipe Detail

Figure 20. Mesh of Welded Stiffener-to-Support Frame Pipe Detail in the Bottom Saddle Connection

In the model used for analyzing the weld connecting the support plate to the support frame pipe in the top and the bottom saddle connections, the plate, the pipe, and the welds were created as one part. The key-hole style notch was again used at the weld root. The mesh size at the notch was 0.01 inch, and the mesh size in the direction perpendicular to the cross-section was set to be 0.04 inch. The elements had regular shapes near the notch. The regions further away from the weld being analyzed were assigned a mesh size of 0.4 inch. The mesh used for the bottom saddle connection is presented in Figure 21.

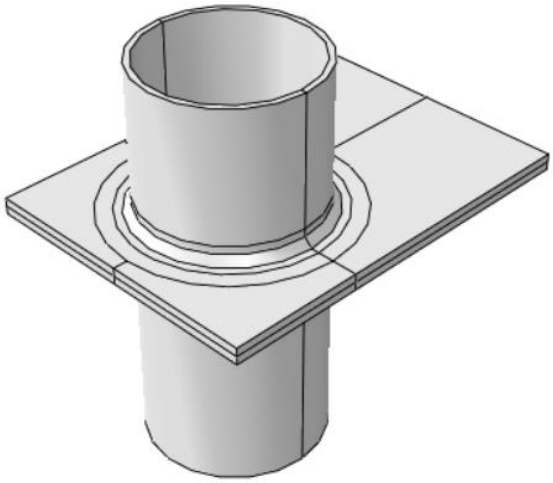

(a) Support Frame Pipe-to-Support Plate Detail

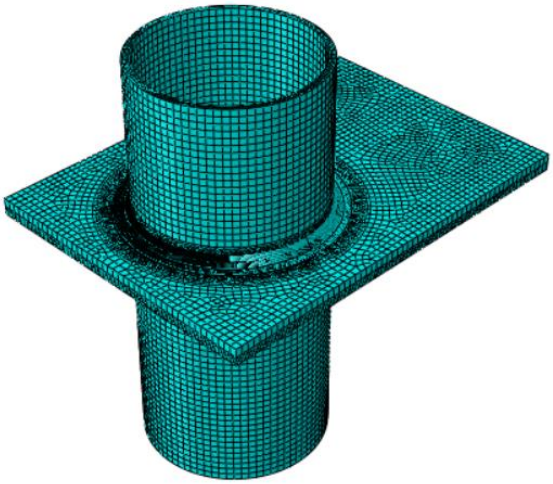

(b) Mesh of Support Frame Pipe-to-Support Plate Detail

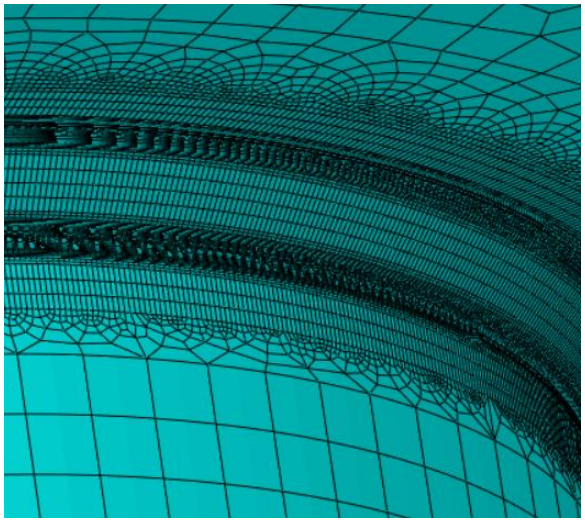

(c) Transition between Fine and Coarse Elements

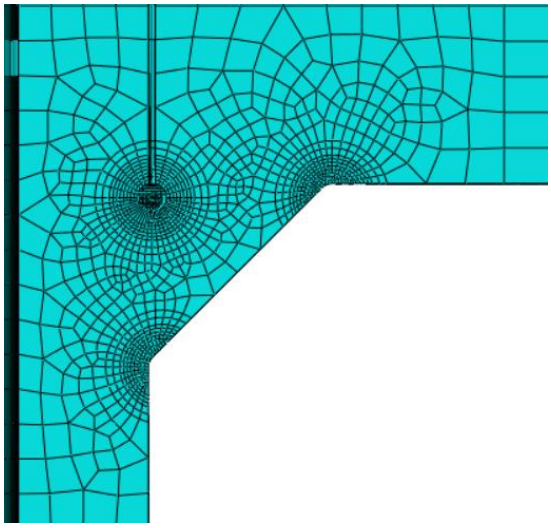

(d) Mesh at Cross-Section of Welded Support Plate to Support Frame Pipe Detail

Figure 21. Welded Support Frame Pipe to Support Plate Detail of Bottom Saddle Connection

The geometry and mesh used for the top saddle connection detail is presented in Figure 22.

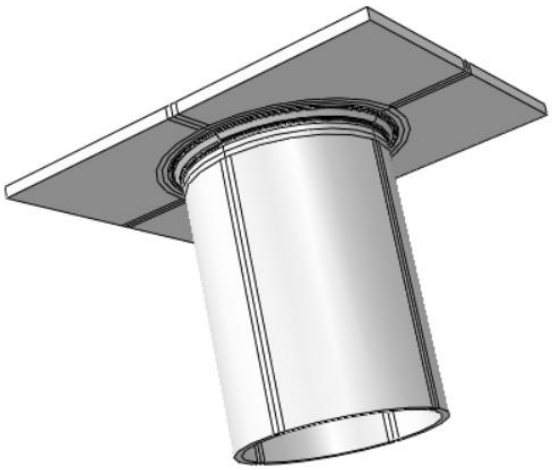

(a) Support Frame Pipe-to-Support Plate Detail

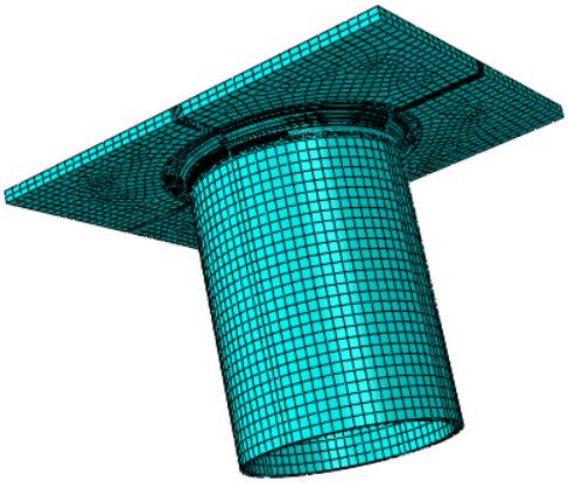

(b) Mesh of Support Frame Pipe-to-Support Plate Detail

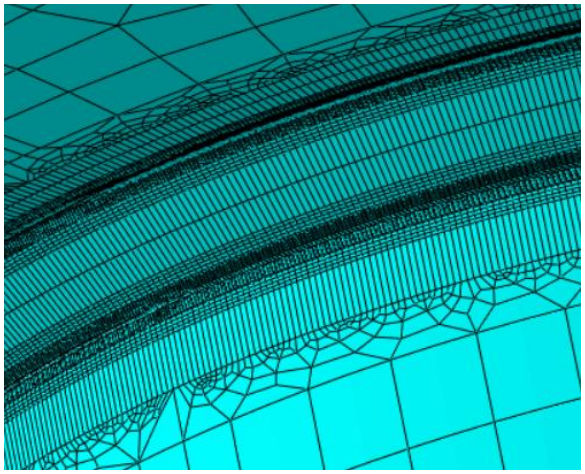

(c) Transition between Fine and Coarse Elements

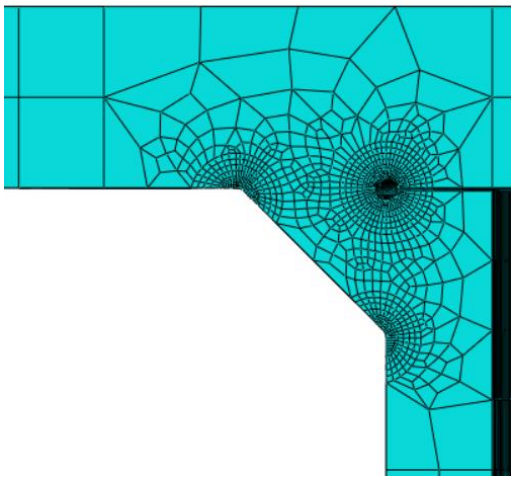

d) Mesh at Cross-Section of Welded Support Plate to Support Frame Pipe Detail

Figure 22. Welded Support Frame Pipe to Support Plate Detail of Top Saddle Connection

Quadratic 20-node solid elements with reduced integration (C3D20R) were used throughout the details. The other solid element parts were created using linear 8-node solid elements (C3D8R).

5.2 Analysis Results

Maximum principal stresses at the surfaces of the notches were extracted and used as the effective notch stresses. Contour plots showing the cross-sections of the welded details at the

locations where peak effective notch stresses were found to be located are presented in Figure 23. For the weld connecting the pipe and the stiffener, the peak maximum principal stress was located at the weld root, with a value of 9.5 ksi. For the welds connecting the support plates and the support frame pipes, the peak maximum principal stresses were found to be 2.1 ksi and 1.3 ksi in the bottom and the top connections respectively, and both were located at the weld toes on the pipes.

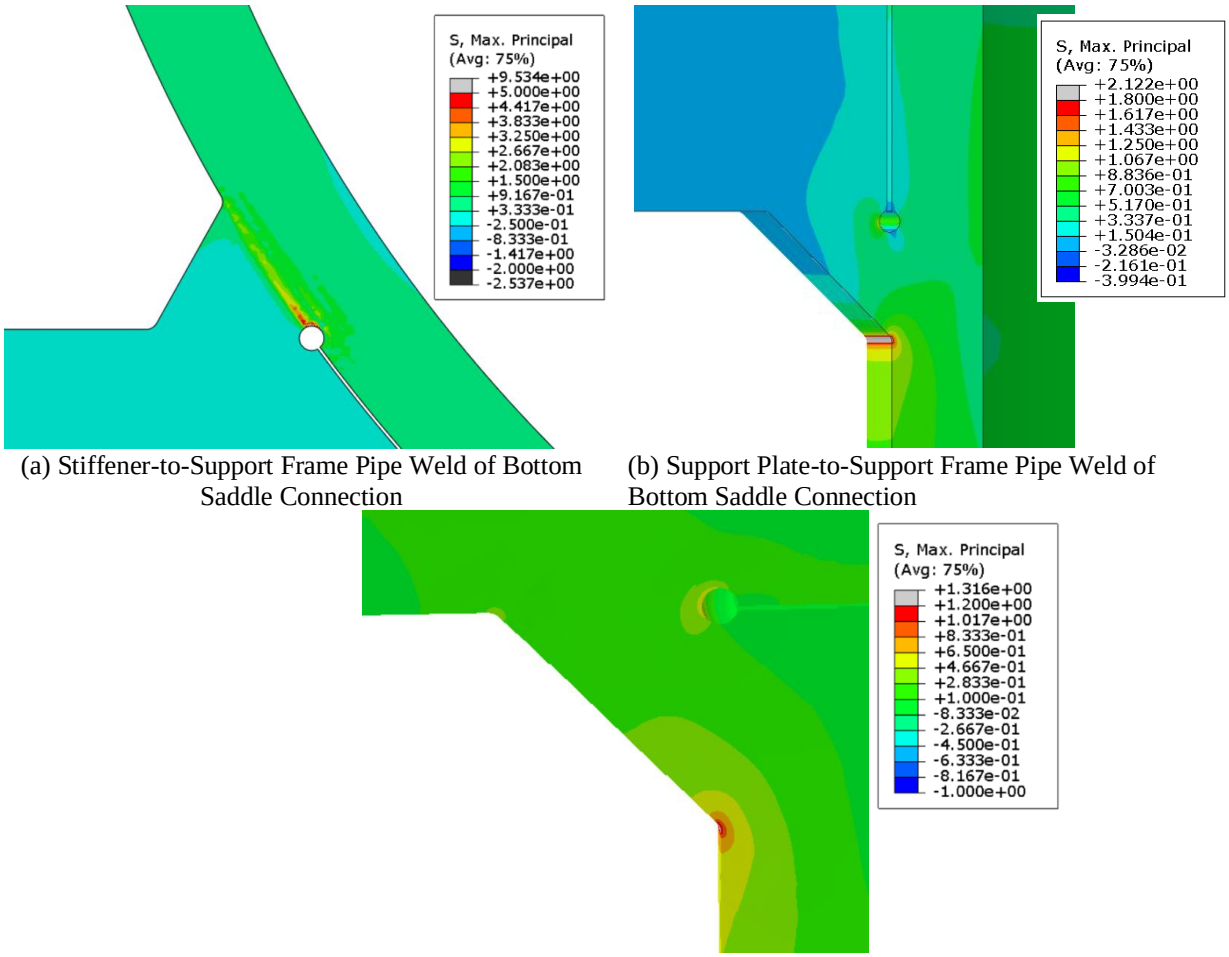

(a) Stiffener-to-Support Frame Pipe Weld of Bottom Saddle Connection

(b) Support Plate-to-Support Frame Pipe Weld of Bottom Saddle Connection

(c) Support Plate to Support Frame Pipe Weld fo Top Saddle Connection

Figure 23. Contour Plots Showing Welded Detail Cross-Sections Where Peak Maximum Principal Stresses Were Located in Effective Notch Stress Analysis

According to AASHTO (2009), corresponding resistance can be determined as $(\Delta F)_l = \frac{1}{3.2}\left[-F_y + \sqrt{{F_y}^2 + 4{F_u}^2}\right]$, with F_y the material yield strength and F_u the ultimate tensile strength, both in ksi. Assuming F_y = 39 ksi and F_u = 45 ksi for aluminum, the calculated resistance is 18.5

ksi. As introduced previously, IIW recommends that its FAT 71 resistance curve be used for aluminum, and DNV includes no recommendation for aluminum. Therefore, resistance curves from AASHTO and IIW provisions have been plotted in Figure 24. All stresses computed using the Effective Notch Stress method were lower than the resistance calculated according to AASHTO, however, the Effective Notch Stress for the weld connecting the stiffener and the pipe did fall above the knee point of the IIW curve.

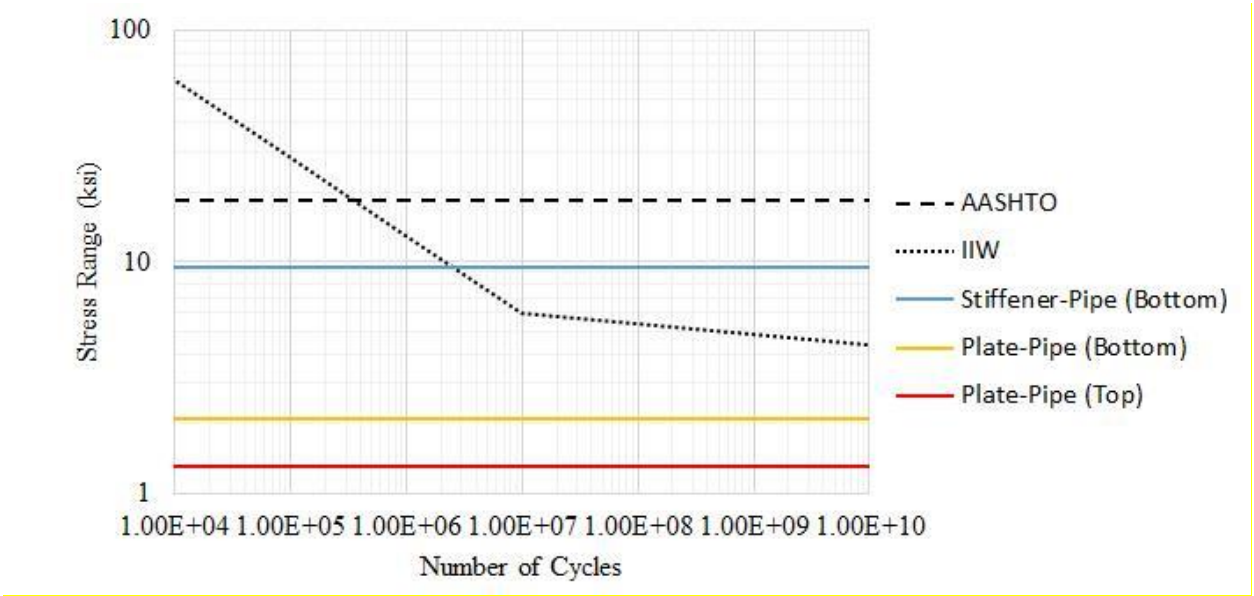

Figure 24. Effective Notch Stress vs. AASHTO and IIW Resistance Curves

Based on these findings, fatigue failures of the saddle connections are not considered likely. However, attention should be pay to the stiffener-to-pipe welds at the bottom saddle connection, as this was the detail found to have the greatest susceptibility.

6. Part Four: Ultimate Strength Behavior of OHTSS Saddle Connections

The saddle connections and the overhead truss sign structures were analyzed to characterize their ultimate strength behavior. Two series of analyses were performed to this end, described in this part of the report. The first was aimed at studying the behavior of the overall structure, and the second focused on analyzing the performance of the saddle connections.

6.1 Model Introduction

6.1.1 Behavior of Overall OHTSS

Models of the overall OHTSS (60-ft and 137-ft spans) were created using 2-node linear beam elements (B31). The truss chords and the support frames were tied together at their joints, simulating moment connections. All degrees-of-freedom at the four support frame ends were restrained to simulate fixed-end boundary conditions. Screen shots of the models are presented in Figure 25.

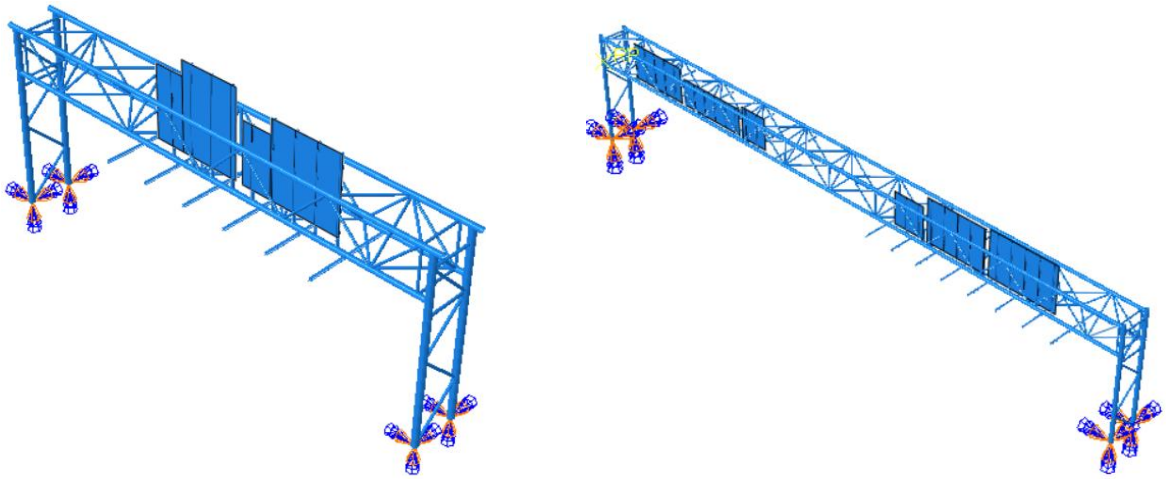

(a) 60-ft Span OHTSS (b) 137-ft Span OHTSS

Figure 25. 60-ft and 137-ft OHTSS Created Using Beam Elements

Elastic-perfectly plastic material properties were used for aluminum, with a modulus of elasticity of 10,000 ksi, Poisson's ratio of 0.35, and a yield strength of 39 ksi. Elastic-perfectly plastic material properties were assigned to all the truss members and the support frames.

The models were loaded until they reached computational limits. In this case, the limits were determined by loss of stiffness due to material yielding. Loading was applied in horizontal, upward, and downward directions. The loads were applied as line loads on truss chords and support frame columns, as shown in Figure 26.

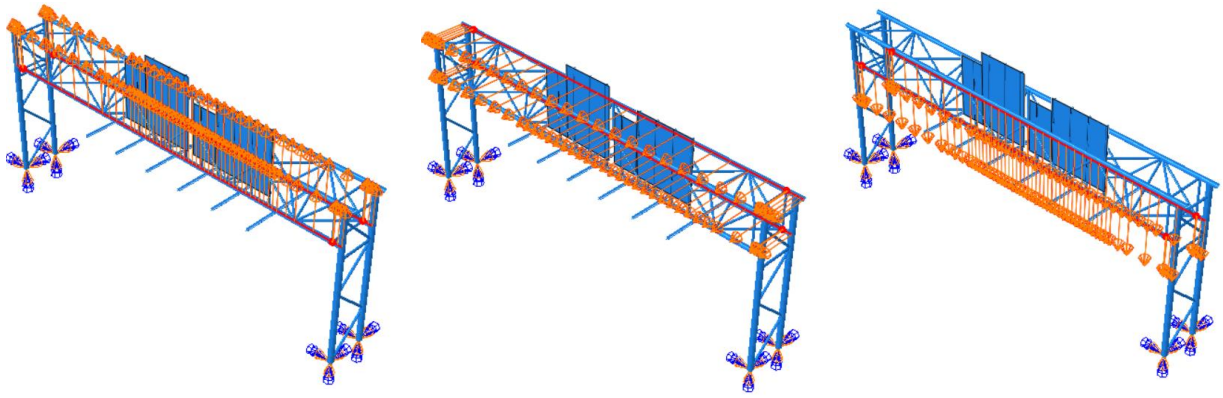

(a) Upward Load (b) Horizontal Load (c) Downward Load

Figure 26. Loads Applied on Overhead Truss Sign Structure for Ultimate Strength Analysis

6.1.2 Performance of Saddle Connections

In the second analysis, 8-node linear 3D solid elements (C3D8R) were used to create models of detailed saddle connections. These models were modified from the models created for the HSS analyses described in Part Two. In the bottom saddle connection models, all DOFs on the surfaces at the top and the bottom of the support frame pipes were restrained, as shown in Figure 27. In the models of the top saddle connection, all DOFs at the bottom surface of the support frame pipe were restrained, as shown in Figure 27.

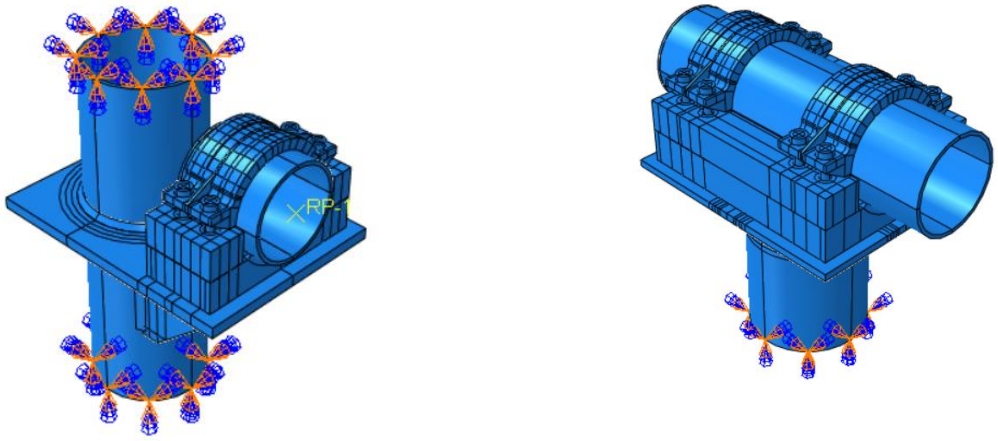

(a) Bottom Saddle Connection (b) Top Saddle Connection

Figure 27. Bottom and Top Saddle Connection Models for Extreme Loading Analyses

Elastic-perfectly plastic material properties were used for aluminum, with a modulus of elasticity of 10,000 ksi, Poisson's ratio of 0.35, and a yield strength of 39 ksi. These properties were assigned to the support plates, support frame pipes, stiffeners, and all of the welds. The other members were assigned linear-elastic properties identical to those described in Part Two. The interaction and contact properties were the same as those introduced in Part Two.

The models were loaded until they reach computational limits. In this case, the limits were determined by loss of stiffness due to material yielding. Loading was applied in downward, upward, horizontal, and axial directions with respect to the direction of the truss chord. The loads were applied as concentrated loads on selected nodes, having an overall effect similar to a pressure load. The axial load was applied on the nodes of the truss chord cross-section. The downward, upward, and horizontal loads were applied at the nodes on the chord where the chord and coupler interact, as shown in Figure 28.

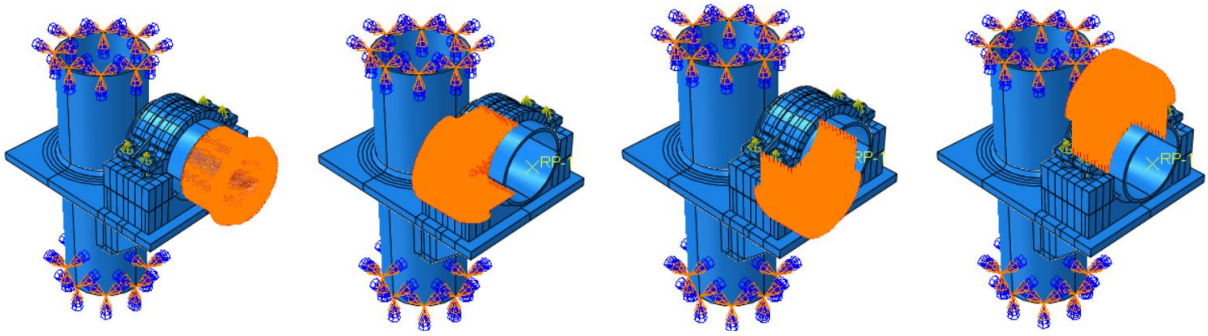

(a) Axial Load (b) Horizontal Load (c) Downward Load (d) Upward Load

Figure 28. Loads Applied on Saddle Connections for Extreme Loading Analysis

6.2 Analysis Results

This part offers a comparison of the behavior of the overall OHTSS and the saddle connections, and provides comments on the performance of the saddle connections at the ultimate strength limit state. However, it is important to note that: 1) the material properties were idealized as elastic-perfectly plastic relationship, and 2) the interactions between members were assumed, for example, the interaction between the keepers and the couplers or chords was simplified with tie constraints.

6.2.1 Behavior of Overall OHTSS

The analysis of the 60-ft OHTSS terminated at a total load of 177 kips, when loaded horizontally. Yielding of the diagonal struts in the supporting frame was found to be the limiter. When the load was applied in the upward and downward directions, analysis terminated at 340 kips, limited by yielding in the diagonal struts in the end panels of the horizontal truss. The contour plots at the end of the analyses are shown in Figure 29. Section forces were output at the joints of support frame pipes and truss chords, and are given in Table 8.

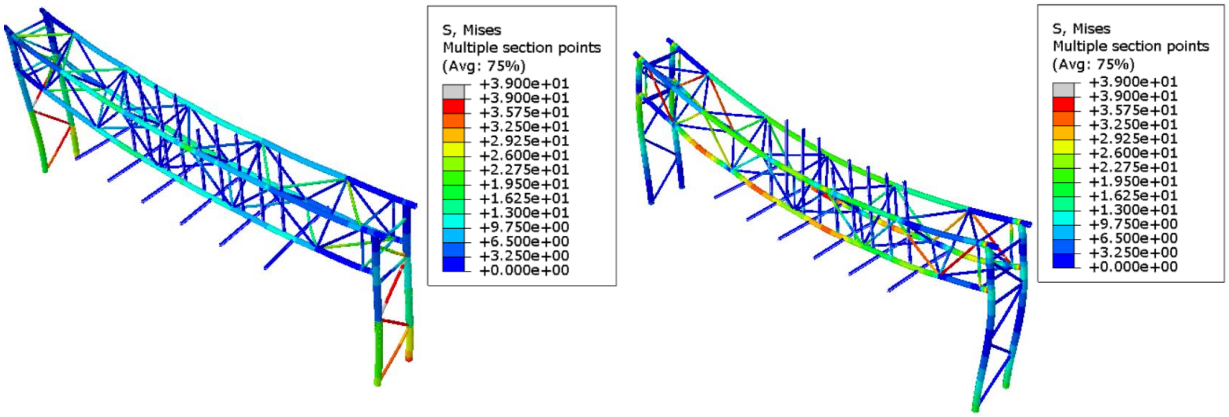

(a) Horizontal Loading (b) Downward Loading

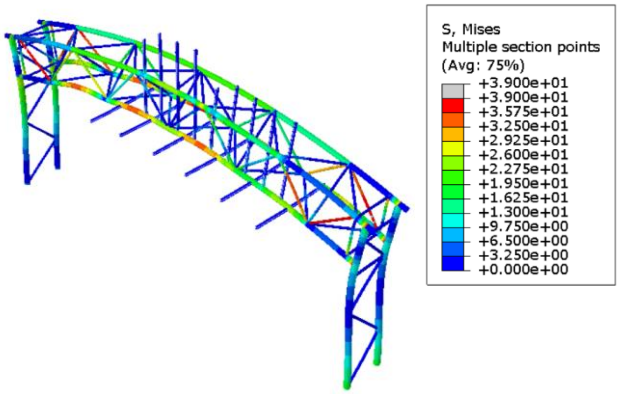

(c) Upward Loading

Figure 29. 60-ft OHTSS at Analysis Termination

Table 8. Section Forces from 60-ft OHTSS at Analysis Termination

Connection	Horizontal Loading (kip)			Vertical Loading (kip)		
	Axial	In-plane	Out-of-plane	Axial	In-plane	Out-of-plane
B1	5.47	11.22	28.71	7.61	47.24	1.89
T1	1.36	6.98	17.80	11.33	40.33	2.05
B2	4.83	12.93	31.45	6.63	45.95	1.21
T2	0.80	5.27	10.82	10.92	36.71	1.05
B3	5.23	11.45	27.85	8.08	47.20	1.36
T3	1.36	6.83	17.54	11.96	40.99	1.56
B4	4.64	12.92	32.49	6.64	45.67	0.84
T4	0.84	5.36	10.70	10.77	35.58	0.63

The analysis of the 137-ft OHTSS terminated at a total load of 180 kips when loaded horizontally, and was controlled by yielding of the middle chords. When the load was applied in the upward and downward directions, analysis terminated at 137 kips, controlled by yielding of the chords at the middle of the horizontal truss. Contour plots showing von Mises stresses at the end of the analyses are shown in Figure 30. Section forces were output at the joints of support frame pipes and truss chords, and are given in Table 8.

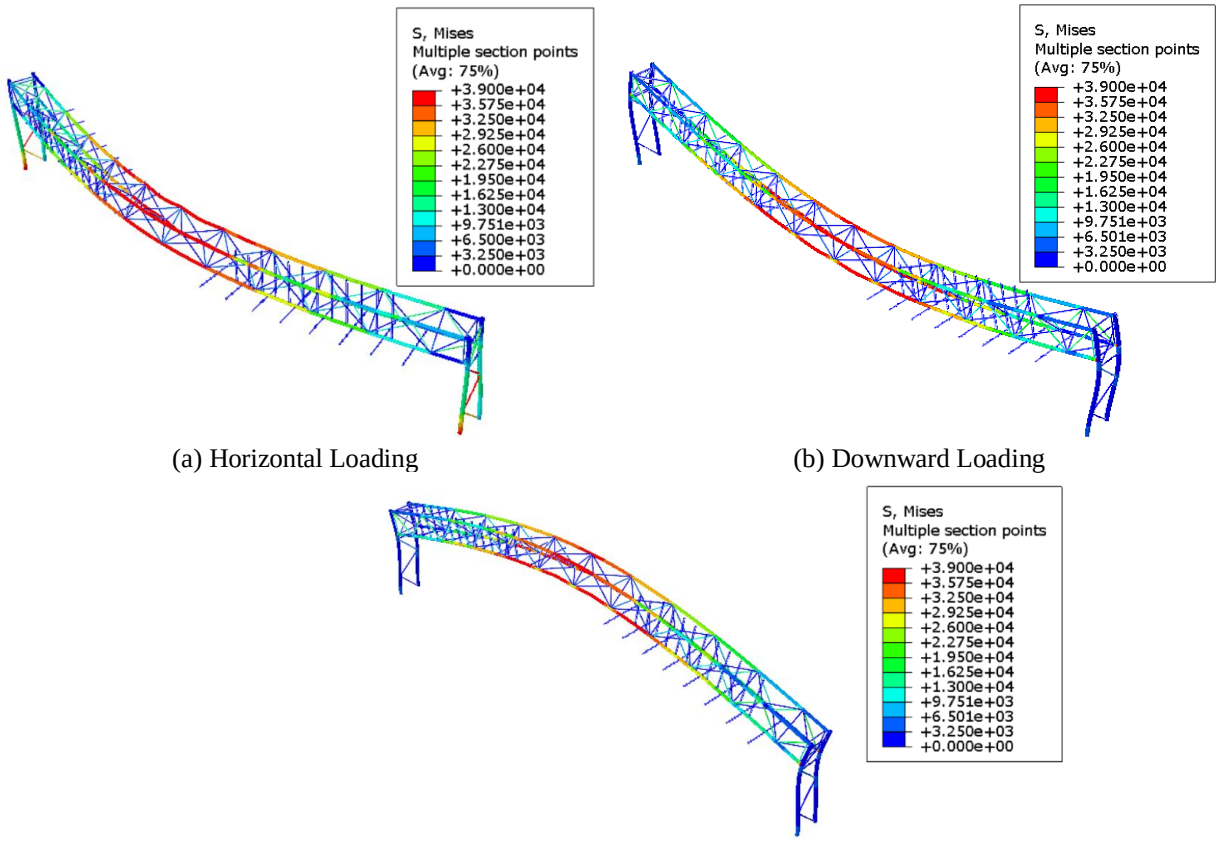

(a) Horizontal Loading

(b) Downward Loading

(c) Upward Loading

Figure 30. 137-ft OHTSS at Analysis Termination

Table 9. Section Forces from 137-ft OHTSS at Analysis Termination

Connection	Horizontal Loading (kip)			Vertical Loading (kip)		
	Axial	In-Plane	Out-of-Plane	Axial	In-Plane	Out-of-Plane
B1	6.10	16.97	33.07	30.43	45.32	0.60
T1	2.60	6.98	9.22	16.92	2.63	0.26
B2	5.96	24.69	33.98	30.71	53.38	0.40
T2	2.60	0.75	13.26	17.78	3.48	0.74
B3	6.69	17.53	33.17	30.11	45.11	0.62
T3	2.78	6.98	9.12	16.60	2.65	0.27
B4	6.52	25.38	34.04	30.33	53.18	0.41
T4	2.75	0.87	13.19	17.40	3.38	0.77

6.2.2 Performance of Saddle Connections

The load-displacement relationships determined for the bottom saddle connection under horizontal, upward, downward, and axial loads are presented in Figure 31 to Figure 34. The two red circles indicate the loads and displacements when localized yielding just started and when global plastic behavior occurred. The global plastic behavior in the models subjected to horizontal,

upward, and downward loads can be clearly noticed as occurring on the linear portion of the load-displacement curves. However, this behavior was not the same for the axially-loaded model, as shown in Figure 34. Here, global plastic behavior was determined as having occurred when the majority of the vertical welds yielded.

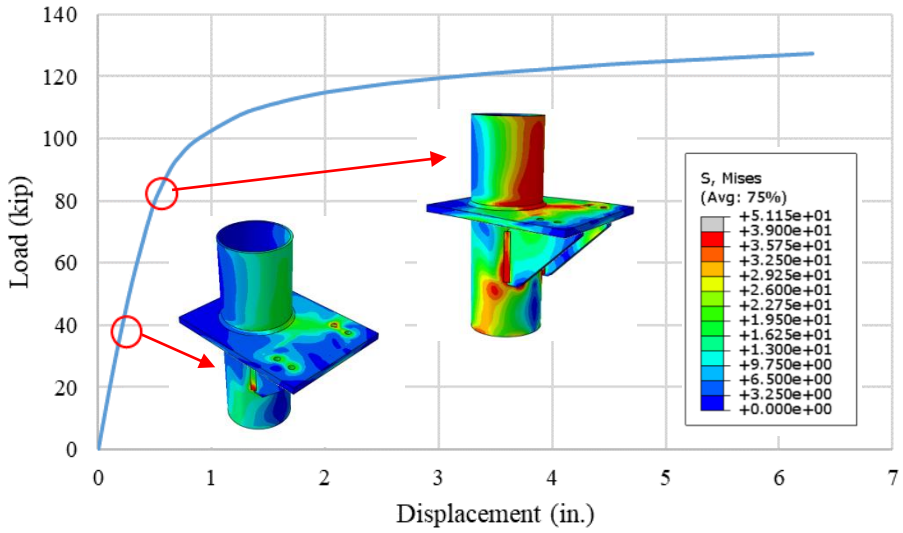

Figure 31. Load-Displacement Behavior for Bottom Saddle Connection under Horizontally Applied Load

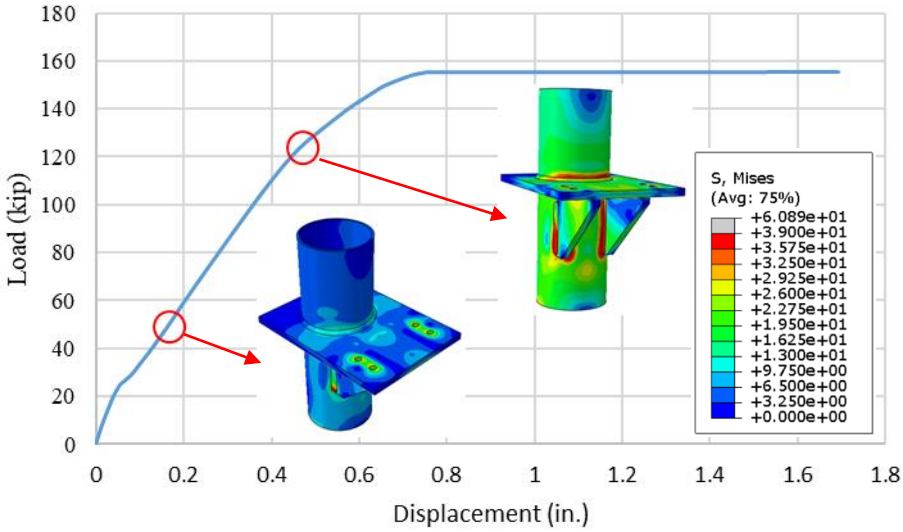

Figure 32. Load-Displacement Behavior for Bottom Saddle Connection under Upwardly Applied Load

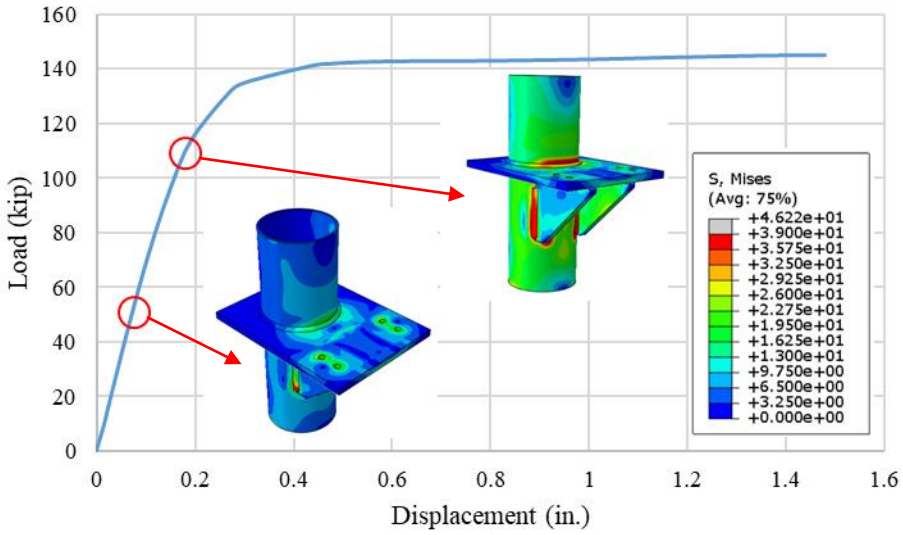

Figure 33. Load-Displacement Behavior for Bottom Saddle Connection under Downwardly Applied Load

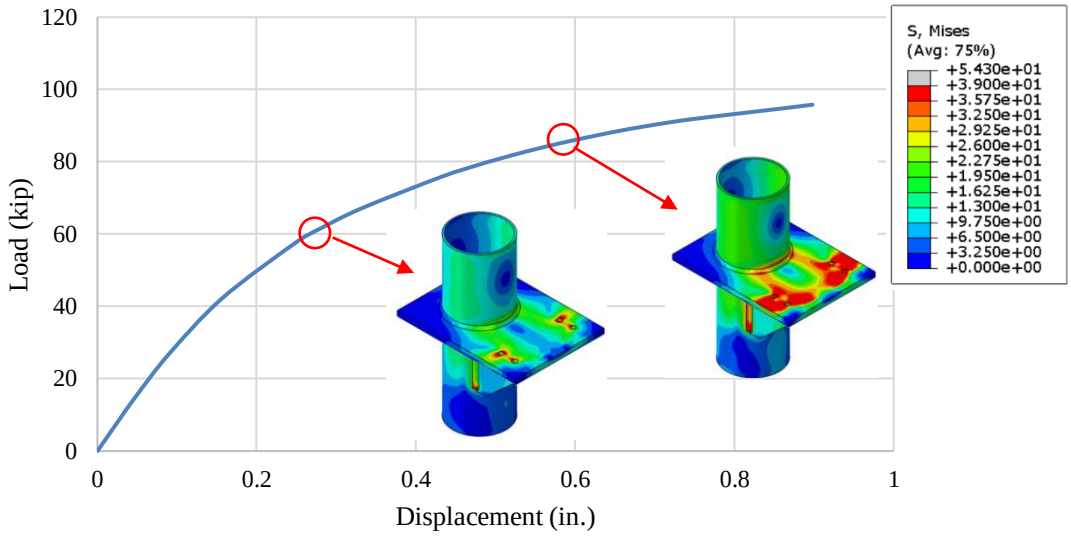

Figure 34. Load-Displacement Behavior for Bottom Saddle Connection under Axially Applied Load

The loads at which the localized yielding occurred, global plastic behavior occurred, and the analysis terminated are summarized in Table 10.

Table 10. Summary of Loads at Starts of Localized Yielding and Global Plastic Behavior of Bottom Saddle Connection

	Horizontal (kip)	Upward (kip)	Downward (Kip)	Axial (kip)
Localized Yielding	37	48	46	58

Global Plastic Behavior	85	125	110	85
Termination Load	127	156	145	96

The load-displacement relationship for the top saddle connection under horizontal, upward, downward, and axial applied loads are presented in Figure 35 to Figure 38. These were loaded until the analyses terminated. In the model in which the load was applied downwardly, 203 kips were applied, but the connection still behaved linearly. This analysis was ended at 203 kips because failure of the model would be governed by overall yielding of the vertical pipe in compression.

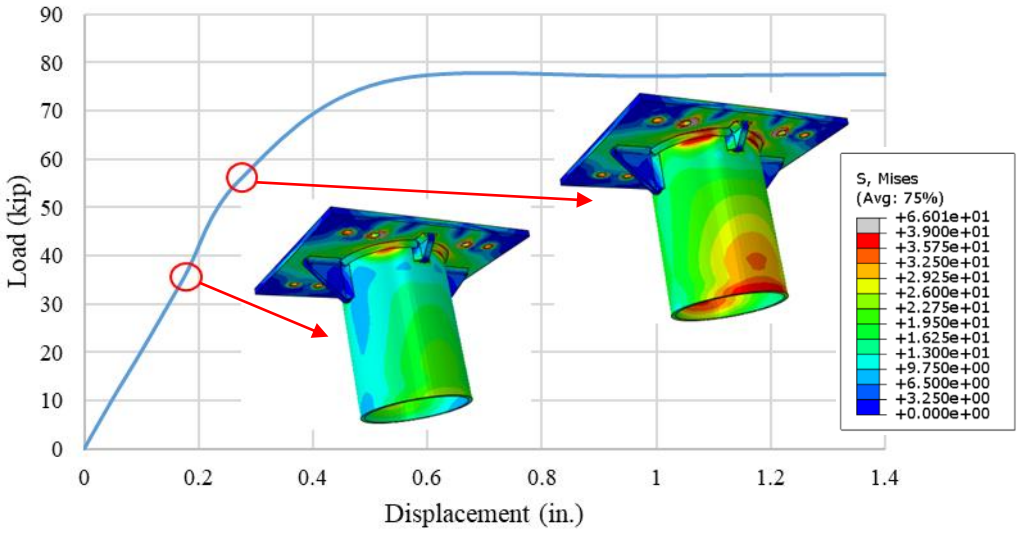

Figure 35. Load-Displacement Behavior for Top Saddle Connection under Horizontal Applied Load

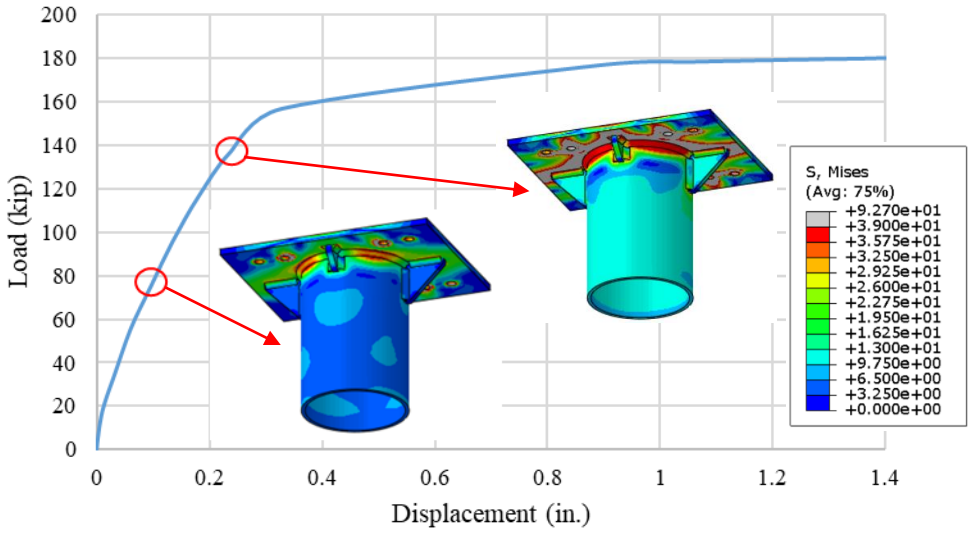

Figure 36. Load-Displacement Behavior for Top Saddle Connection under Upward Applied Load

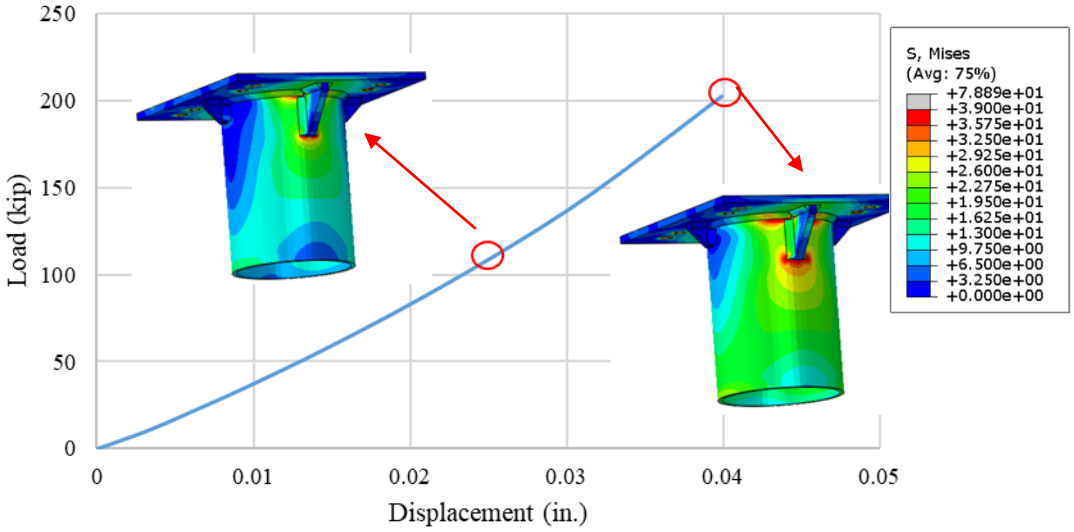

Figure 37. Load-Displacement Behavior for Top Saddle Connection under Downward Applied Load

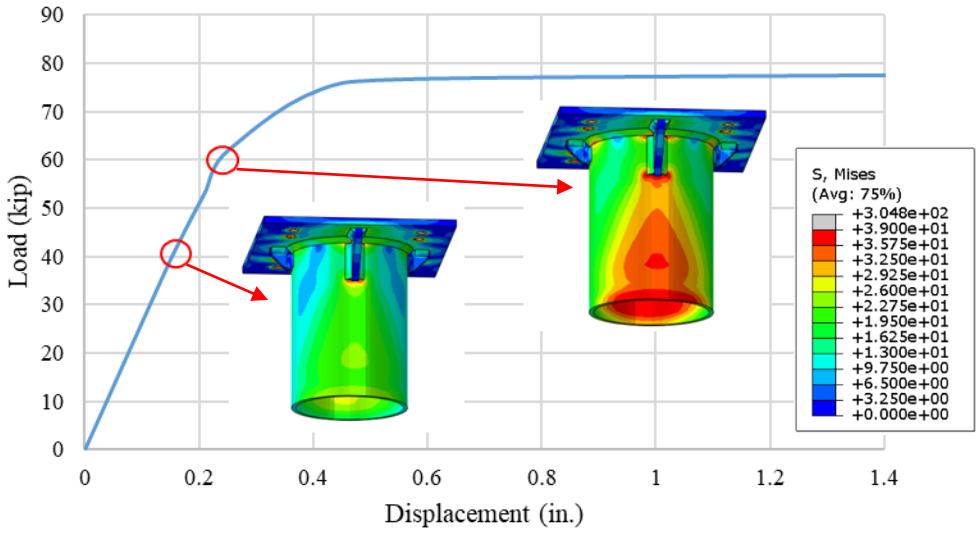

Figure 38. Load-Displacement Behavior for Top Saddle Connection under Axial Applied Load

Table 11. Summary of Loads at Start of Localized Yielding and Global Plastic Behavior of Top Saddle Connection

	Horizontal (kip)	Upward (kip)	Downward (Kip)	Axial (kip)
Localized Yielding	35	76	117	40
Global Plastic Behavior	56	137	Analysis ended at 203 kip. No global plastic behavior occurred yet.	62
Termination Load	78	181	Analysis ended at 203 kip. Analysis did not terminated due to material yielding.	79

Most of the section forces that were found to occur at termination of the overall OHTSS models were smaller than the loads at which the localized yielding commenced in the saddle connection models. An interaction equation can be used to determine the safety of the saddle connections, as shown in (Equation 3, relating the behavior of the saddle connection to that of the overall OHTSS. The loads corresponding to the start of global plastic behavior were used in the calculations. For the denominator, the vertical load was taken as the smaller one between upward and downward applied loads.

$$\sum \frac{Section\ Force\ at\ Connection\ at\ Analysis\ Termination\ of\ Overall\ Structure}{Applied\ Load\ in\ Saddle\ Connection\ Analysis\ at\ Start\ of\ Global\ Plastic\ Behavior} \leq 1$$

(Equation 3)

The results for each connection have been summarized in Table 12. The calculation results for all the connections were found to be smaller than one, suggesting that at the failure of the overall structure, the saddle connections may not have reached diffused plastic behavior. Therefore, ultimate strength of the OHTSS is not likely to be governed by strength of the saddle connections.

Table 12. Interaction Equation Calculation of Section Forces at Connections, at Point of Analysis Termination for the Overall OHTSS

Connection	60 ft Structure		137 ft Structure	
	Horizontal Loading	Vertical Loading	Horizontal Loading	Vertical Loading
B1	0.50	0.54	0.62	0.78
T1	0.39	0.51	0.26	0.30
B2	0.54	0.51	0.69	0.85
T2	0.24	0.46	0.28	0.33
B3	0.49	0.54	0.63	0.77
T3	0.39	0.52	0.26	0.29
B4	0.55	0.50	0.71	0.85
T4	0.24	0.44	0.29	0.32

7. Conclusions

This study was focused on evaluating the fatigue susceptibility of saddle connections used in new Kansas DOT OHTSS. Four series of finite element analyses have been presented in this report, including: (1) a series of analyses to determine the global behavior of OHTSS for selecting critical connections; (2) a study using Structural Hot Spot Stress method; (3) a study using Effective Notch Stress method; (4) and an analysis characterizing the relative performance of the sign structures and the saddle connections for ultimate strength. The primary conclusions are summarized as follows:

- The bottom saddle connections were found to have larger Structural Hot Spot Stresses than the top saddle connections, for all span lengths included in the study.
- The AASHTO (2009) design loads corresponding to natural wind loads blowing in the direction perpendicular to the sign panel were found to almost always produce the largest stress ranges in the saddle connections.
- The Structural Hot Spot Stresses were found to all be below the constant fatigue threshold of the AASHTO resistance curve. In addition, the largest HSS was below the knee point of DNV and IIW curves and intersected the two curves at approximately 10^8 cycles and 10^{11} cycles. Overall, these results indicate that fatigue failures are unlikely to occur.
- For the three welds analyzed using the Effective Notch Stress method, the peak effective notch stresses all occurred below the resistance determined using AASHTO (2009). However, the peak Effective Notch Stress at the weld root of the stiffener-pipe weld of the bottom saddle connection occurred above the knee point of the IIW resistance curve. Overall, the AASHTO-based results indicate that fatigue failures are unlikely to occur, however, the stiffener-pipe weld should be considered as the most susceptible location for fatigue susceptibility.
- The stiffener-to-pipe welds on the bottom saddle connections corresponded to larger stress ranges in both Structural Hot Spot Stress analysis and Effective Notch Stress analysis than other welds in the saddle connection assemblies.

- Fatigue failures of the saddle connections are considered unlikely in expected real use. However, attention should be paid to the stiffener-to-pipe welds of the bottom saddle connection, and high levels of fabrication quality should be ensured.
- Analysis results for the OHTSS and saddle connections suggest that at the point of failure of the overall OHTSS, the saddle connections may not have even reached the starting point of diffused plastic behavior. Therefore, strength of OHTSS was found to not be governed by ultimate strength of the saddle connections.

References

AASHTO. (2009). Standard Specifications for Structural Supports for Highway Signs, Luminaires and Traffic Signals. (5th ed.). American Association of State Highway Transportation Officials, Washington, D.C.

Dexter, R.J. and Ricker, M.J. (2002). NCHRP Report 469: Fatigue-Resistant Design of Cantilevered Signal, Sign, and Light Supports. Transportation Research Board of the National Academies, Washington, D.C.

DNV. (2011). Recommended Practice DNV-RP-C203: Fatigue Design of Offshore Steel Structures. Det Norske Veritas AS.

Fam, A., Witt, S., and Rizkalla, S. (2006). "Repair of damaged aluminum truss joints of highway overhead sign structures using FRP." Construction and Building Materials, 20(10), 948–956.

Fouad, F.H., Davidson, J.S., Delatte, N., Calvert, E.A., Chen, S., Nunez, E., and Abdalla, R. (2003). NCHRP Report 494: Structural Supports for Highway Signs, Luminaires, and Traffic Signals. Transportation Research Board of the National Academies, Washington, D.C.

Foutch, D.A., Rice, S.A., Lafave, J.M., Valdovinos, S., and Kim, T.W. (2006). FHWA/IL/PRR 153: Evaluation of Aluminum Highway Sign Trusses and Standards for Wind and Truck Gust Loadings. Illinois Department of Transportation, Springfield, Illinois.

Fricke, W. (2010). IIW-Doc. XIII-2240r2-08/XV-1289r2-08: IIW Recommendations for the Fatigue Assessment by Notch Stress Analysis for Welded Structures. Hamburg University of Technology, Germany.

Fricke, W. (2012). IIW-Doc. XIII-2380r3-11/XV-1383r3-11: IIW Guideline for the Assessment of Weld Root Fatigue. Hamburg University of Technology, Germany.

Hobbacher, A. (2008). Recommendations for fatigue design of welded joints and Components. IIW Doc XIII-2151r1-07/XV-1254r1-07. International Institute of Welding, Paris, France.

Kacin, J., Rizzo, P., and Tajari, M. (2010). "Fatigue Analysis of Overhead Sign Support Structures." Engineering Structures, 32(6), 1659–1670.

Niemi, E., Fricke, W., and Maddox, S.J. (2018). Fatigue Analysis of Welded Components: Designers Guide to the Structural Hot Spot Stress Approach. Springer, Singapore.

Rice, J. A., Foutch, D. A., Lafave, J. M., and Valdovinos, S. (2012). "Field testing and analysis of aluminum highway sign trusses." Engineering Structures, 34, 173–186.

Yang, S., King, J., and Hong, H. (2020). "Validation of fatigue design wind loads for natural wind gusts and for truck-induced wind gusts using full-scale measurements." Journal of Wind Engineering and Industrial Aerodynamics, 198, 104084.